Studying gaugino mass unification at the LHC

JHEP04(2009)114

(http://iopscience.iop.org/1126-6708/2009/04/114)

JHEP

Published by IOP Publishing for SISSA

Received: *February 4, 2009*
Accepted: *April 6, 2009*
Published: *April 28, 2009*

Studying gaugino mass unification at the LHC

Baris Altunkaynak,[a] **Phillip Grajek,**[b] **Michael Holmes,**[a] **Gordon Kane**[b] **and Brent D. Nelson**[a]

[a] *Department of Physics, Northeastern University, Boston, MA, 02115 U.S.A.*
[b] *Michigan Center for Theoretical Physics, Randall Lab., University of Michigan, Ann Arbor, MI 48109, U.S.A.*
E-mail: altunkaynak.i@neu.edu, phillip.grajek@umich.edu, holmes.mi@neu.edu, gkane@umich.edu, b.nelson@neu.edu

Abstract: We begin a systematic study of how gaugino mass unification can be probed at the CERN Large Hadron Collider (LHC) in a quasi-model independent manner. As a first step in that direction we focus our attention on the theoretically well-motivated mirage pattern of gaugino masses, a one-parameter family of models of which universal (high scale) gaugino masses are a limiting case. We improve on previous methods to define an analytic expression for the metric on signature space and use it to study one-parameter deviations from universality in the gaugino sector, randomizing over other soft supersymmetry-breaking parameters. We put forward three ensembles of observables targeted at the physics of the gaugino sector, allowing for a determination of this non-universality parameter without reconstructing individual mass eigenvalues or the soft supersymmetry-breaking gaugino masses themselves. In this controlled environment we find that approximately 80% of the supersymmetric parameter space would give rise to a model for which our method will detect non-universality in the gaugino mass sector at the 10% level with $\mathcal{O}(10\ \text{fb}^{-1})$ of integrated luminosity. We discuss strategies for improving the method and for adding more realism in dealing with the actual experimental circumstances of the LHC.

Keywords: Supersymmetry Phenomenology, Strings and branes phenomenology

ArXiv ePrint: 0901.1145

doi:10.1088/1126-6708/2009/04/114

JHEP04(2009)114

Contents

JHEP04(2009)114

1 Introduction

As the Large Hadron Collider (LHC) era fast approaches, the theoretical community is increasingly focused on how the new discoveries made there will be interpreted. The first step, most obviously, is to establish the presence of physics beyond the Standard Model. This will be done using search strategies that are by now well-established, though many interesting "what-if" scenarios continue to be proposed and investigated [1]. We continue to believe that supersymmetry (SUSY) is the best-motivated extension to the Standard Model for physics at the LHC energy scale. Furthermore, if supersymmetry is indeed relevant at the electroweak scale there are many reasons to expect that its presence will be established early on in the LHC program [2]. Indeed, even some properties of the spectrum, such as the masses and spins of low-lying new states, may be crudely known even after relatively little integrated luminosity [3–5]. In this paper we begin a research program into what comes next: how to connect the multiple LHC observations to organizing principles in some (high-energy) effective Lagrangian of underlying physics.

This secondary problem can be further divided into two sub-problems. The first has come to be called the "inversion" problem. Briefly stated, the inversion problem is the

recognition that even in very restrictive model frameworks it is quite likely that more than one set of model parameters will give predictions for LHC observations that are in good agreement with the experimental data [6]. Much recent work has focused on how to address this issue [7–11], and we will borrow much of the philosophy and many of the useful techniques from this recent literature. But our focus here is on what we might call the second sub-problem: how to turn the ensemble of distinct LHC signatures into a determination of certain broad properties of the underlying Lagrangian at low energies. Clearly the most direct attack on this second sub-problem is to perform a global fit to the parameters of a particular model [12, 13], modulo the degeneracy issue just described above. Not surprisingly, therefore, the work we will describe in this paper will make significant use of likelihood fits. But our ultimate goal is to fit to certain broad properties of the *underlying physics itself* — and not simply to a particular model of that physics.

We will refine this rather vague-sounding goal in a moment. But it is helpful to first consider an example of what we mean by the phrase "broad properties of the underlying physics." Consider a high energy theorist interested in connecting the (supersymmetric) physics at the LHC to physics at an even higher energy scale, such as some underlying string theory. What sort of information would be of most use to him or her in this pursuit? Would it be a precise measurement of the gluino mass, or of the mass splitting in the top squark sector, or some other such measurement? Obtaining such information is (at least in principle) possible at the LHC, but far more valuable would be knowledge of the size of the supersymmetric μ-parameter or whether $\tan\beta$ is very small. Such information is far more difficult to obtain at the LHC [14] but is more correlated with moduli stabilization and/or how the μ-parameter is generated in string models [15]. For example, this knowledge may tell us whether the μ-parameter is fundamental in the superpotential or generated via the Kähler potential as in the Giudice-Masiero mechanism [16]. This, in turn, is far more powerful in discriminating between potential string constructions than the gluino mass itself — no matter how accurately it is determined. We might refer to the genesis of the μ-parameter as a "broad property of the underlying physics."

If all such key broad properties of the underlying physics were enumerated, it is our view that one of the most important such properties would be the question of gaugino mass universality. That is, the notion that at the energy scale at which supersymmetry breaking is transmitted to the observable sector, the gauginos of the minimal supersymmetric Standard Model (MSSM) all acquired soft masses of the same magnitude. This issue is intimately related to another, perhaps equally important issue: the wave-function of the lightest supersymmetric particle, typically the lightest neutral gaugino. Few properties of the superpartner spectrum have more far-reaching implications for low-energy phenomenology, the nature of supersymmetry breaking, and the structure of the underlying physics Lagrangian [17]. If the theorist could be told only one "result" from the LHC data the answer to the simple question "Is there evidence for gaugino mass universality?" might well be it. But these soft parameters are not themselves directly measurable at the LHC [18].[1] One might consider performing a fit to some particular theory, such as

[1]Even a measurement of the physical gluino mass is not a direct measurement of the associated SU(3)

JHEP04(2009)114

minimal supergravity (mSUGRA), in which universal gaugino masses are assumed [21] — or perhaps to certain models with fixed, non-universal gaugino mass ratios [22, 23]. But we are not so much interested in whether mSUGRA — or any other particular theory for which gaugino mass universality is a feature — is a good fit to the data. Rather, we wish to know whether gaugino mass universality is a property of the underlying physics *independent of all other properties of the model.* From this example both the ambitiousness and the difficulty inherent in our task is clear.

We have therefore decided to begin our attack by considering a concrete parametrization of non-universalities in soft gaugino masses. Many such frameworks present themselves, but we will choose a parametrization that has the virtue of also having a strong theoretical motivation from string theory. In recent work by Choi and Nilles [24] soft supersymmetry-breaking gaugino mass patterns were explored in a variety of string-motivated contexts. In particular, the so-called "mirage pattern" of gaugino masses provides an interesting case study in gaugino mass non-universality. Yet as mentioned above, these soft supersymmetry breaking parameters are not themselves directly measurable. Linking the soft parameters to the underlying Lagrangian is important, but without the crucial step of linking the parameters to the data itself it will be impossible to reconstruct the underlying physics from the LHC observations.

The mirage paradigm gets its name from the fact that should the mirage pattern of gaugino masses be used as the low-energy boundary condition of the (one-loop) renormalization group equations then there will exist some high energy scale at which all three gaugino masses are identical. This unification has nothing to do with grand unification of gauge groups, however, and the gauge couplings will in general *not* unify at this particular energy scale — hence the name "mirage." The set of all such low-energy boundary conditions that satisfy the mirage condition defines a one-parameter family of models. This parameter can be taken to be the mirage unification scale itself, or some other parameter, such as the ratio between various contributions to the gaugino soft masses. We note that the minimal supergravity paradigm of soft supersymmetry breaking is itself a member of this family of models since it is *defined* by the property that gaugino masses are universal at the scale $M_{\rm GUT} \simeq 2 \times 10^{16}$ GeV. Indeed, in the parametrization we adopt from [24], the gaugino mass ratios at the electroweak scale take the form

$$M_1 \,:\, M_2 \,:\, M_3 \,\simeq\, (1 + 0.66\alpha) \,:\, (2 + 0.2\alpha) \,:\, (6 - 1.8\alpha)\,, \tag{1.1}$$

where the case $\alpha = 0$ is precisely the unified mSUGRA limit. Note that when we speak of testing gaugino mass universality, therefore, we do not imagine a common gaugino soft mass at the low-energy scale. Instead, the "universality" paradigm implies the ratios

$$M_1 \,:\, M_2 \,:\, M_3 \simeq 1 \,:\, 2 \,:\, 6\,. \tag{1.2}$$

The goal of this work is to ask whether it is possible to determine that the α parameter of (1.1) is different from zero — and if so, how.

soft mass M_3. Quantum corrections to the gluino bare mass can be sizable and their theoretical computation involves a large set of other MSSM soft parameters [19, 20] — which are also not directly measurable!

JHEP04(2009)114

The theoretical details behind the ratios of (1.1) will be the topic of section 2 in this paper. These details are largely irrelevant for the analysis that follows in sections 3 and 4, but may nevertheless be of interest to many readers. For those who are only interested in the methodology we will pursue and the results, this section can be omitted. At the end of section 2 we will present two benchmark scenarios that arise from concrete realizations of the mirage pattern of gaugino masses in certain classes of string models. As this is a paper about the interface of theory and experiment at the LHC — and not about string phenomenology per se – we will leave the theoretical description of these models to the appendix. In section 3 we discuss how we will go about attempting to measure the value of the parameter α in (1.1) and describe the process that led us to an ensemble of specific LHC observables targeted for precisely this purpose. In section 4 this list of signatures is tested on a large collection of MSSM models, as well as on our two special benchmarks from section 2. We will see that the signature lists constructed using the method of section 3 do an excellent job of detecting the presence of non-universality in the gaugino soft masses over a very wide array of supersymmetric spectra hierarchies and mass ranges. Non-universality on the order of 30-50% should become apparent within the first 10 fb^{-1} of analyzed data for most supersymmetric models consistent with current experimental constraints. Detecting non-universality at the 10% level would require an increase in data by roughly a factor of two. Nevertheless, depending on the details of the superpartner spectrum, some cases will require far more data to truly measure the presence of non-universality. Of course all of these statements must here be understood in the context of the very particular assumptions of this study. Some thoughts on how the process can be taken further in the direction of increased realism are discussed in the concluding section.

Before moving to the body of the paper, however, we would like to take a moment to emphasize a few broad features of the theoretical motivation behind the parametrization in (1.1). In the limit of very large values for the parameter α the ratios among the gaugino masses approach those of the anomaly-mediated supersymmetry breaking (AMSB) paradigm [25, 26]. In fact, the mirage pattern is most naturally realized in scenarios in which a common contribution to all gaugino masses is balanced against an equally sizable contribution proportional to the beta-function coefficients of the three Standard Model gauge groups. Such an outcome arises in string-motivated contexts, such as KKLT-type moduli stabilization in D-brane models [27, 28] and Kähler stabilization in heterotic string models [29]. These string-derived manifestations can also be extended easily to include the presence of gauge mediation, in which the mirage pattern is maintained in the gaugino sector [30, 31]. Importantly, however, it can arise in *non*-stringy models, such as deflected anomaly mediation [32, 33]. We note that in none of these cases is the pure-AMSB limit likely to be obtained, so our focus here will be on small to moderate values of the parameter α in (1.1).[2] We will further refine these observations in section 2 before turning our attention to the measurement of the parameter α at the LHC.

[2]In any event, the phenomenology of the AMSB scenario is sufficiently distinct from the models we will consider that distinguishing between them should not be difficult [34].

JHEP04(2009)114

2 Theoretical motivation and background

In this section we wish to understand the origin of the mass ratios in (1.1) from first principles. We will treat the mirage mass pattern here in complete generality, without any reference to its possible origin from string-theoretic considerations. This short section concludes with two specific sets of soft parameters, both of which represent models with the mirage gaugino mass pattern (though the physics behind the rest of their soft supersymmetry breaking parameters are quite different). In the appendix we will recast the discussion of this section in terms of the degrees of freedom present in low-energy effective Lagrangians from string model building. There we will also present the string theory origin of the two benchmark models that appear in table 1 at the end of this section.

Let us begin by imagining a situation in which there are two contributions to the soft supersymmetry breaking gaugino masses. We assume that these contributions arise at some effective high-energy scale at which supersymmetry breaking is transmitted from some hidden sector to the observable sector. Let us refer to this scale as simply the ultraviolet scale $\Lambda_{\rm UV}$. It is traditional in phenomenological treatments to take this scale to be the GUT scale at which gauge couplings unify, but in string constructions one might choose a different (possibly higher scale) at which the supergravity approximation for the effective Lagrangian becomes valid. We will further assume that one contribution to gaugino masses is universal in nature while the other contribution is proportional to the beta-function coefficient of the Standard Model gauge group. More specifically, consider the universal piece to be given by

$$M_a^1\left(\Lambda_{\rm UV}\right) = M_u\,, \tag{2.1}$$

where $a = 1, 2, 3$ labels the Standard Model gauge group factors $\mathcal{G}_a$ and M_u represents some mass scale in the theory. The second piece is the so-called anomaly mediated piece, which arises from loop diagrams involving the auxiliary scalar field of supergravity [35, 36]. It will take the form

$$M_a^2\left(\Lambda_{\rm UV}\right) = g_a^2\left(\Lambda_{\rm UV}\right)\frac{b_a}{16\pi^2}M_g\,, \tag{2.2}$$

where the b_a are the beta-function coefficients for the Standard Model gauge groups. In our conventions these are given by

$$b_a = -(3C_a - \sum_i C_a^i), \tag{2.3}$$

where C_a, C_a^i are the quadratic Casimir operators for the gauge group $\mathcal{G}_a$, respectively, in the adjoint representation and in the representation of the matter fields Φ^i charged under that group.[3] For the MSSM these are

$$\{b_1, b_2, b_3\} = \left\{\frac{33}{5}, 1, -3\right\}\,. \tag{2.4}$$

Note that if we take $\Lambda_{\rm UV} = \Lambda_{\rm GUT}$ then we have

$$g_1^2\left(\Lambda_{\rm UV}\right) = g_2^2\left(\Lambda_{\rm UV}\right) = g_3^2\left(\Lambda_{\rm UV}\right) = g_{\rm GUT}^2 \simeq \frac{1}{2}\,. \tag{2.5}$$

[3] The convention chosen in (2.3) is opposite of the one chosen in [37].

JHEP04(2009)114

The mass scale M_g is common to all three gauge groups; the subscript is meant to indicate that the contribution in (2.2) is related to the gravitino mass. The full gaugino mass at the high energy boundary condition scale is therefore

$$M_a\left(\Lambda_{\rm UV}\right) = M_a^1\left(\Lambda_{\rm UV}\right) + M_a^2\left(\Lambda_{\rm UV}\right) = M_u + g_a^2\left(\Lambda_{\rm UV}\right)\frac{b_a}{16\pi^2}M_g\,. \tag{2.6}$$

Now imagine evolving the boundary conditions in (2.6) to some low-energy scale $\Lambda_{\rm EW}$ via the (one-loop) renormalization group equations (RGEs). For the anomaly-generated piece of (2.2) we need only replace the gauge coupling with the value at the appropriate scale

$$M_a^2\left(\Lambda_{\rm EW}\right) = g_a^2\left(\Lambda_{\rm EW}\right)\frac{b_a}{16\pi^2}M_g\,, \tag{2.7}$$

while for the universal piece we can use the fact that M_a/g_a^2 is a constant for the one-loop RGEs. After some manipulation this yields

$$M_a^1\left(\Lambda_{\rm EW}\right) = M_u\left[1 - g_a^2\left(\Lambda_{\rm EW}\right)\frac{b_a}{8\pi^2}\ln\left(\frac{\Lambda_{\rm UV}}{\Lambda_{\rm EW}}\right)\right]\,. \tag{2.8}$$

Combining (2.8) and (2.7) gives the low scale expression

$$M_a\left(\Lambda_{\rm EW}\right) = M_u\left\{1 - g_a^2\left(\Lambda_{\rm EW}\right)\frac{b_a}{8\pi^2}\ln\left(\frac{\Lambda_{\rm UV}}{\Lambda_{\rm EW}}\right)\left[1 - \frac{1}{2}\frac{M_g}{M_u\ln\left(\frac{\Lambda_{\rm UV}}{\Lambda_{\rm EW}}\right)}\right]\right\}\,. \tag{2.9}$$

For gaugino masses to be unified *at the low scale* $\Lambda_{\rm EW}$ then the quantity in the square brackets in (2.9) must be engineered to vanish. This can be achieved with a judicious choice of the values M_u and M_g for a particular high-energy input scale $\Lambda_{\rm UV}$. Put differently, for a given $\Lambda_{\rm UV}$ (such as the GUT scale) and a given overall scale M_u, there is a one-parameter family of models defined by the choice M_g.

It is possible, however, to find a more convenient parametrization of the family of gaugino mass patterns defined by (2.9). Consider defining the parameter α by

$$\alpha = \frac{M_g}{M_u\ln\left(\Lambda_{\rm UV}/\Lambda_{\rm EW}\right)}\,, \tag{2.10}$$

so that (2.9) becomes

$$M_a\left(\Lambda_{\rm EW}\right) = M_u\left[1 - \left(1 - \frac{\alpha}{2}\right)g_a^2\left(\Lambda_{\rm EW}\right)\frac{b_a}{8\pi^2}\ln\left(\frac{\Lambda_{\rm UV}}{\Lambda_{\rm EW}}\right)\right] \tag{2.11}$$

and the requirement of universality at the scale $\Lambda_{\rm EW}$ now implies $\alpha = 2$. Normalizing the three gaugino masses by $M_1\left(\Lambda_{\rm EW}\right)|_{\alpha=0}$ and evaluating the gauge couplings at a scale $\Lambda_{\rm EW} = 1000$ GeV we obtain the mirage ratios

$$M_1 \,:\, M_2 \,:\, M_3 \;=\; (1.0 + 0.66\alpha) \,:\, (1.93 + 0.19\alpha) \,:\, (5.87 - 1.76\alpha)\,, \tag{2.12}$$

for $\Lambda_{\rm UV} = \Lambda_{\rm GUT}$, in good agreement with the expression in (1.1).

Let us generalize the parametrization in (2.10) once more. Instead of defining the parameter in terms of the starting and stoping points in the RG evolution of the gaugino

JHEP04(2009)114

mass parameters, we will fix them in terms of mass scales in the theory itself. Thus we follow the convention of Choi et al. [38] and define

$$\alpha \equiv \frac{M_g}{M_u \ln\left(M_{\rm PL}/M_g\right)}\,, \tag{2.13}$$

where $M_{\rm PL}$ is the reduced Planck mass $M_{\rm PL} = 2.4 \times 10^{18}$ GeV. Our parametrization is now divorced from the boundary condition scales of the RG flow and can be fixed in advance. The choice of mass parameters in the logarithm of (2.13) may seem arbitrary — and at this point it is indeed completely arbitrary — but they have been chosen so as to make better contact with string constructions, such as those which we present in the appendix. Inserting (2.13) into (2.9) yields

$$\begin{aligned} M_a\left(\Lambda_{\rm EW}\right) &= M_u \left\{1 - g_a^2\left(\Lambda_{\rm EW}\right)\frac{b_a}{8\pi^2}\left[\ln\left(\frac{\Lambda_{\rm UV}}{\Lambda_{\rm EW}}\right) - \frac{\alpha}{2}\ln\left(\frac{M_{\rm PL}}{M_g}\right)\right]\right\} \\ &= M_u \left\{1 - g_a^2\left(\Lambda_{\rm EW}\right)\frac{b_a}{8\pi^2}\left[\ln\left(\frac{\Lambda_{\rm UV}\left(M_g/M_{\rm PL}\right)^{\alpha/2}}{\Lambda_{\rm EW}}\right)\right]\right\}. \end{aligned} \tag{2.14}$$

Comparing this expression with (2.8) it is clear if gauge couplings unify at a scale $\Lambda_{\rm UV} = \Lambda_{\rm GUT}$, then we should expect the soft supersymmetry breaking gaugino masses to unify at an effective scale given by

$$\Lambda_{\rm mir} = \Lambda_{\rm GUT}\left(\frac{M_g}{M_{\rm PL}}\right)^{\alpha/2}. \tag{2.15}$$

We see that our parametrization in terms of α is indeed equivalent to a parametrization in terms of the effective unification scale, as suggested in the introduction.

The value of α as defined in (2.10) or (2.13) can be crudely thought of as the ratio of the anomaly contribution to the universal contribution to gaugino masses. Indeed, the limit $\alpha \to 0$ is the limit of the minimal supergravity paradigm, while $\alpha \to \infty$ is the AMSB limit. But as (2.6) makes clear, these two contributions will be of comparable size only if M_g is at least an order of magnitude larger than M_u. We could therefore have chosen a parametrization based on the ratio $r = M_g/M_u$, with interesting values being in the range $r \simeq \mathcal{O}(10 - 100)$. But such a parametrization spoils the simple relation with the mirage unification scale (2.15). Furthermore, the introduction of the factor $\ln(M_{\rm PL}/M_g)$ in (2.13) provides the needed large factor, taking a value of $\ln(M_{\rm PL}/M_g) \simeq 35$ for $M_g \simeq 1\,\text{TeV}$. To obtain the mirage pattern it is therefore necessary for the underlying theory to generate some large number $c \simeq \ln(M_{\rm PL}/M_g) \simeq 30$. Specific examples of how this is achieved in explicit string-based models are given in the appendix to this paper.

In table 1 we have collected the necessary soft supersymmetry-breaking parameters to completely specify two benchmark points for further analysis in what follows. The details behind these two models are described in appendix A. Here we will simply indicate that point A represents a heterotic string model with Kähler stabilization of the dilaton which was studied in detail in [37]. This particular example has a value of $\alpha = 0.3$. Point B is an example from a class of Type IIB string compactifications with fluxes which was studied in [38]. This second example has a value $\alpha = 1.0$. Both are examples of the mirage

JHEP04(2009)114

Parameter	Point A	Point B		Parameter	Point A	Point B
α	0.3	1.0		$m^2_{Q_3}$	$(1507)^2$	$(430.9)^2$
M_g	1.5 TeV	16.3 TeV		$m^2_{U_3}$	$(1504)^2$	$(610.3)^2$
M_1	198.7	851.6		$m^2_{D_3}$	$(1505)^2$	$(352.2)^2$
M_2	172.1	553.3		$m_{\tilde{c}_R}$, $m^2_{L_3}$	$(1503)^2$	$(381.6)^2$
M_3	154.6	339.1		$m^2_{E_3}$	$(1502)^2$	$(407.9)^2$
A_t	193.0	1309		$m^2_{Q_{1,2}}$	$(1508)^2$	$(208.4)^2$
A_b	205.3	1084		$m^2_{U_{1,2}}$	$(1506)^2$	$(302.7)^2$
A_τ	188.4	1248		$m^2_{D_{1,2}}$	$(1505)^2$	$(347.0)^2$
$m^2_{H_u}$	$(1500)^2$	$(752.0)^2$		$m^2_{L_{1,2}}$	$(1503)^2$	$(379.8)^2$
$m^2_{H_d}$	$(1503)^2$	$(388.7)^2$		$m^2_{E_{1,2}}$	$(1502)^2$	$(404.5)^2$

Table 1. **Soft Term Inputs**. Initial values of supersymmetry breaking soft terms in GeV at the initial scale given by $\Lambda_{\rm UV} = 2 \times 10^{16}$ GeV. Both points are taken to have $\mu > 0$ and $\tan\beta = 10$. The actual value of $\tan\beta$ is fixed in the electroweak symmetry-breaking conditions.

pattern of gaugino masses, having mirage unification scales of $\Lambda_{\rm mir} = 2.0 \times 10^{14}$ GeV and $\Lambda_{\rm mir} = 1.5 \times 10^{9}$ GeV, respectively. Note that these soft supersymmetry breaking terms are taken to be specified at the GUT energy scale of $\Lambda_{\rm GUT} = 2.0 \times 10^{16}$ GeV and must be evolved to electroweak scale energies through the renormalization group equations.

3 Determining α: methodology

3.1 Setting up the problem

As mentioned in the introduction, the ultimate goal of this avenue of study is to determine whether or not soft supersymmetry breaking gaugino masses obey some sort of universality condition independent of all other facts about the supersymmetric model. Such a goal cannot be met in a single paper so we have begun by asking a simpler question: *assuming* the world is defined by the MSSM with gaugino masses obeying the relation (1.1), how well can we determine the value of the parameter α. At the very least we would like to be able to establish that $\alpha \neq 0$ with a relatively small amount of integrated luminosity. The first step in such an incremental approach is to demonstrate that some set of "targeted observables" [12] (we will call them "signatures" in what follows) is sensitive to small changes in the value of the parameter α in a world where all other parameters which define the SUSY model are kept fixed. In subsequent work we intend to relax this strong constraint and treat the issue of gaugino mass universality more generally. Despite the lack of realism we feel this is a logical point of departure — very much in the spirit of the "slopes" of the Snowmass Points and Slopes [39] and other such benchmark studies. Thus, where the Snowmass benchmarks talk of slopes, we will here speak of "model lines" in which all parameters are kept fixed but the value of α is varied in a controlled manner.

To construct a model line we must specify the supersymmetric model in all aspects other than the gaugino sector. The MSSM is completely specified by 105 distinct parame-

JHEP04(2009)114

ters, but only a small subset are in any way relevant for the determination of LHC collider observables [14]. We will therefore choose a simplified set of 17 parameters as in the two benchmark models of table 1

$$\left\{ \begin{array}{c} \tan\beta,\ m^2_{H_u},\ m^2_{H_d} \\ M_3,\ A_t,\ A_b,\ A_\tau \\ m_{Q_{1,2}},\, m_{U_{1,2}},\, m_{D_{1,2}},\, m_{L_{1,2}},\, m_{E_{1,2}} \\ m_{Q_3},\, m_{U_3},\, m_{D_3},\, m_{L_3},\, m_{E_3} \end{array} \right\} . \tag{3.1}$$

The parameters in (3.1) are understood to be taken at the electroweak scale (specifically $\Lambda_{\rm EW} = 1000$ GeV) so no renormalization group evolution is required. The gluino soft mass M_3 will set the overall scale for the gaugino mass sector. The other two gaugino masses M_1 and M_2 are then determined relative to M_3 via (2.12). A model line will take the inputs of (3.1) and then construct a family of theories by varying the parameter α from $\alpha = 0$ (the mSUGRA limit) to some non-zero value in even increments.

For each point along the model line we pass the model parameters to `PYTHIA 6.4` [40] for spectrum calculation and event generation. Events are then sent to the `PGS4` [41] package to simulate the detector response. Additional details of the analysis will be presented in later sections. The end result of our procedure is a set of observable quantities that have been designed and (at least crudely) optimized so as to be effective at separating $\alpha = 0$ from other points along the model line in the least amount of integrated luminosity possible. In section 3.2 we describe the manner in which we perform this separation between models. The signature lists, and the analysis behind their construction, is presented in section 3.3. Throughout both of these sub-sections we will make reference to certain statistical material contained in appendix B. In section 4 we will demonstrate the effectiveness of these signature lists on a large sample of randomly generated model lines and provide some deeper insight on why the whole procedure works by examining our benchmarks in greater detail.

3.2 Distinguishability

The technique we will employ to distinguish between candidate theories using LHC observables was suggested in [12] and subsequently refined in [6]. The basic premise is to construct a variable similar to a traditional chi-square statistic

$$(\Delta S_{AB})^2 = \frac{1}{n} \sum_i \left[\frac{S_i^A - S_i^B}{\delta S_i^{AB}} \right]^2 , \tag{3.2}$$

where S is some observable quantity (or signature). The index $i = 1, \ldots, n$ labels these signatures, with n being the total number of signatures considered. The labels A and B indicate two distinct theories which give rise to the signature sets S_i^A and S_i^B, respectively. Finally, the error term δS_i^{AB} is an appropriately-constructed measure of the uncertainty of the term in the numerator, i.e. the difference between the signatures. In this work we will always define a signature S as an observation interpreted as a count (or number) and denote it with capital N. One example is the number of same-sign, same-flavor lepton pairs in a

JHEP04(2009)114

certain amount of integrated luminosity. Another example is taking the invariant mass of all such pairs and forming a histogram of the results, then integrating from some minimum value to some maximum value to obtain a number. In principle there can be an infinite number of signatures defined in this manner. In practice experimentalists will consider a finite number and many such signatures are redundant.

We can identify any signature N_i with an effective cross section $\bar{\sigma}_i$ via the relation

$$\bar{\sigma}_i = N_i/L\,, \tag{3.3}$$

where L is the integrated luminosity. We refer to this as an *effective* cross-section as it is defined by the counting signature N_i which contains in its definition such things as the geometric cuts that are performed on the data, the detector efficiencies, and so forth. Furthermore these effective cross sections, whether inferred from actual data or simulated data, are subject to statistical fluctuations. As we increase the integrated luminosity we expect that this effective cross section $\bar{\sigma}_i$ (as inferred from the data) converges to an "exact" cross section σ_i given by

$$\sigma_i = \lim_{L\to\infty} \bar{\sigma}_i\,. \tag{3.4}$$

These exact cross sections are (at least in principle) calculable predictions of a particular theory, making them the more natural quantities to use when trying to distinguish between theories. The transformation in (3.3) allows for a comparison of two signatures with differing amounts of integrated luminosity. This will prove useful in cases where the experimental data is presented after a limited amount of integrated luminosity L_A, but the simulation being compared to the data involves a much higher integrated luminosity L_B. Using these notions we can re-express our chi-square variable $(\Delta S_{AB})^2$ in terms of the cross sections

$$(\Delta S_{AB})^2 = \frac{1}{n}\sum_i \left[\frac{\bar{\sigma}_i^A - \bar{\sigma}_i^B}{\delta\bar{\sigma}_i^{AB}}\right]^2\,. \tag{3.5}$$

We will assume that the errors associated with the signatures N_i are purely statistical in nature and that the integrated luminosities L_A and L_B are precisely known, so that

$$\delta\bar{\sigma}_i^{AB} = \sqrt{(\delta\bar{\sigma}_i^A)^2 + (\delta\bar{\sigma}_i^B)^2} = \sqrt{\bar{\sigma}_i^A/L_A + \bar{\sigma}_i^B/L_B}\,, \tag{3.6}$$

and therefore $(\Delta S_{AB})^2$ is given by

$$(\Delta S_{AB})^2 = \frac{1}{n}\sum_i \left[\frac{\bar{\sigma}_i^A - \bar{\sigma}_i^B}{\sqrt{\bar{\sigma}_i^A/L_A + \bar{\sigma}_i^B/L_B}}\right]^2\,, \tag{3.7}$$

where each cross section includes the (common) Standard Model background, i.e. $\bar{\sigma}_i = \bar{\sigma}_i^{\rm SUSY} + \bar{\sigma}^{\rm SM}$.

The variable $(\Delta S_{AB})^2$ forms a measure of the distance between any two theories in the space of signatures defined by the S_i. We can use this metric on signature space to answer the following question: how far apart should two sets of signatures S_i^A and S_i^B be before we conclude that theories A and B are truly distinct? The original criterion used

JHEP04(2009)114

in [6] was as follows. Imagine taking any supersymmetric theory and performing a collider simulation. Now choose a new random number seed and repeat the simulation. Due to random fluctuations we expect that even the same set of input parameters, after simulation and event reconstruction, will produce a slightly different set of signatures. That is, we expect $(\Delta S_{AA})^2 \neq 0$ since it involves the *effective* cross-sections as extracted from the simulated data. Now repeat the simulation a large number of times, each with a different random number seed. Use (3.7) to compute the distance of each new simulation with the original simulation in signature space. The set of all $(\Delta S_{AA})^2$ values so constructed will form a distribution. Find the value of $(\Delta S_{AA})^2\big|_{95}$ in this distribution which represents the 95th percentile of the distribution. This might be taken as a measure of the uncertainty in "distance" measurements associated with statistical fluctuations.

This procedure for defining distinguishability is unwieldy in a number of respects. Determining the threshold for separating models by $(\Delta S_{AB})^2 > (\Delta S_{AA})^2\big|_{95}$ is computationally intensive as it requires many repeated simulations of the same model (as well as the Standard Model background). More importantly, the "brute force" determination of $(\Delta S_{AA})^2\big|_{95}$ is particular to model A as well as the list of signatures used in (3.7). Each change in either the model parameters or the signature mix demands a new determination of the threshold for distinguishability. We will therefore propose a new criterion that has the benefit of being analytically calculable with a form that is universal to any pair of models and any set of signatures. Details behind the criterion can be found in appendix B.

In the limit in which the luminosities L_A and L_B are large the probability distribution for the quantity $(\Delta S_{AB})^2$ given by

$$P(\Delta S^2) = n\,\chi^2_{n,\lambda}(n\Delta S^2)\,, \tag{3.8}$$

where $\chi^2_{n,\lambda}$ is the non-central chi-squared distribution for n degrees of freedom. The non-centrality parameter λ is given by

$$\lambda = \sum_i \frac{(\sigma_i^A - \sigma_i^B)^2}{\sigma_i^A/L_A + \sigma_i^B/L_B}\,, \tag{3.9}$$

and now the σ_i represent *exact* cross sections. From (3.8) and (3.9) it is apparent that all the physics behind the distribution of possible $(\Delta S_{AB})^2$ values is contained in the values of λ and n. In particular the distribution of possible $(\Delta S_{AA})^2$ values (a central chi-square distribution) should depend *only* on the number n of signatures considered — not on the model point nor on the nature of those signatures. In particular, to distinguish a model from itself we must consider (3.8) for the case $\lambda = 0$. If we use the criterion from [6] and require $(\Delta S_{AB})^2 > (\Delta S_{AA})^2\big|_{95\text{th}}$ then we are requiring that $(\Delta S_{AB})^2$ be larger than the 95-th percentile value for the distribution (3.8) for the appropriate n value. This is an analytically computable number which we denote $\gamma_n(95)$. These numbers $\gamma_n(p)$, for various p-th percentiles, are given in table 10 in appendix B.

Now return to the basic problem: using experimental data to distinguish two models that truly are distinct. Though we have $\lambda \neq 0$, there is always a finite chance that an experimental measurement will not reveal this fact due to quantum fluctuations. For any

JHEP04(2009)114

given value of $\lambda \neq 0$, the probability that a measurement of $(\Delta S_{AB})^2$ will fluctuate to a value so small that it is not possible to separate two distinct models (to confidence level p) is simply the fraction of the probability distribution in (3.8) that lies to the left of the value $\gamma_n(p)$. There is always some minimum value of the non-centrality parameter that can be chosen so that this fraction is below some pre-determined value. Let us call that value $\lambda_{\min}(n,p)$. Again, these values are simply determined by integrating the probability distributions (3.8) and are independent of the physics of the problem. A table of these values for various values of n and confidence level p is given in table 11 in appendix B. So, for example, given two distinct models A and B, any combination of n experimental signatures such that $\lambda > \lambda_{\min}(n, p = 0.95)$ will be effective in demonstrating that the two models are indeed different 95% of the time, with a confidence level of 95%.

Let us assume for the moment that "model A" is the experimental data, which corresponds to an integrated luminosity of $L^{\rm exp}$. Our "model B" can then be a simulation with integrated luminosity $L^{\rm sim} = qL^{\rm exp}$. We will make one final notational definition

$$R_{AB} = \sum_i (R_{AB})_i = \sum_i \frac{(\sigma_i^A - \sigma_i^B)^2}{\sigma_i^A + \frac{1}{q}\,\sigma_i^B} \tag{3.10}$$

where R_{AB} has the units of a cross section. Our condition for 95% certainty that we will be able to separate two truly distinct models at the 95% confidence level becomes

$$L_{\rm exp} \geq \frac{\lambda_{\min}(n, 0.95)}{R_{AB}}\,. \tag{3.11}$$

Given two models A and B and a selection of n signatures both $\lambda_{\min}(n, 0.95)$ and R_{AB} are completely determined. Therefore the minimum amount of integrated luminosity needed to separate the models experimentally will be given by

$$L_{\min}(p) = \frac{\lambda_{\min}(n,p)}{R_{AB}}\,. \tag{3.12}$$

We will be using (3.12) repeatedly throughout the rest of this paper. A well-chosen set of signatures will be the set that makes the resulting value of $L_{\min}$ determined from (3.12) as small as it can possibly be.

3.3 Specific signature choice

Following the discussion in section 3.2 we are in a position to define the goal behind our signature selection more precisely. We wish to select a set of n signatures S_i such that the quantity $L_{\min}(p)$ as defined in (3.12), for a given value of p, is as small as it can possibly be over the widest possible array of model pairs A and B. We must also do our best to ensure that the n signatures we choose to consider are reasonably uncorrelated with one another so that the statistical treatment of the preceding section is applicable. We will address the latter issue below, but let us first turn our attention to the matter of optimizing the signature list.

We took as our starting point an extremely large initial set of possible signatures. These included all the counting signatures and most of the kinematic distributions used in [6],

JHEP04(2009)114

all of the signatures of [42], several "classic" observables common in the literature [43] and several more which we constructed ourselves. Removing redundant instances of the same signature this yielded 46 independent counting signatures and 82 kinematic distributions represented by histograms, for 128 signatures in total. We might naively think that the best strategy is to include *all* of these signatures in the analysis (neglecting for now the issue of possible correlations among them). In fact, if the goal is statistically separating two models, the optimal strategy is generally to choose a rather small subset of the total signatures. Let us understand why that is the case. To do so we need a quantitative way of establish an absolute measure of the "power" of any given signature to separate two models A and B. This can be provided by considering the condition in (3.12). For any signature S_i we can define an individual $(L_{\min})_i$ by

$$(L_{\min})_i = \lambda_{\min}(1,p)\,\frac{\sigma_i^A + \frac{1}{q}\,\sigma_i^B}{(\sigma_i^A - \sigma_i^B)^2}\,, \tag{3.13}$$

where, for example, $\lambda_{\min}(1, 0.95) = 12.99$. This quantity is exactly the integrated luminosity required to separate models A and B, to confidence level p, by using the single observable S_i. For a list of N signatures it is possible to construct N such $(L_{\min})_i$ values and order them from smallest value (most powerful) to largest value (least powerful). If we take any subset n of these, then the requisite $L_{\min}$ that results from considering all n simultaneously is given by

$$L_{\min} = \frac{\lambda_{\min}(n,p)}{\lambda_{\min}(1,p)}\,\left\{(L_{\min})_1^{-1} + (L_{\min})_2^{-1} + \cdots + (L_{\min})_n^{-1}\right\}^{-1}\,. \tag{3.14}$$

Referring to the values in table 11 of appendix B, we see that the ratio $\lambda_{\min}(n,p)/\lambda_{\min}(1,p)$ grows with n. This indicates that as we add signatures with ever diminishing $(L_{\min})_i$ values we will eventually encounter a point of negative returns, where the resulting overall $L_{\min}$ starts to grow again.

As more signatures are added, the threshold for adding the next signature in the list gets steadily stronger. For a *particular pair* of models, A and B, it is always possible to find the optimal list of signatures from among a given grand set by ordering the resulting $(L_{\min})_i$ values and adding them sequentially until a minimum of $L_{\min}$ is observed. To do so, we note that kinematic distributions must be converted into counts (and all counts are then converted into effective cross sections). This conversion requires specifying an integration range for each histogram. The choice of this range can itself be optimized, by considering each integration range as a separate signature and choosing the values such that $(L_{\min})_i$ is minimized.

Figure 1, based on an actual pair of models from one of our model lines, represents the outcome of just such an optimization procedure. In this case a clearly optimal signature set is given by the 12 signatures represented by the circled point, which yields $L_{\min} = 2.4\,\text{fb}^{-1}$. The situation in figure 1 is typical of the many examples we studied: the optimal signature set usually consisted of $\mathcal{O}(10)$ signatures. If we are willing to settle for a luminosity just

JHEP04(2009)114

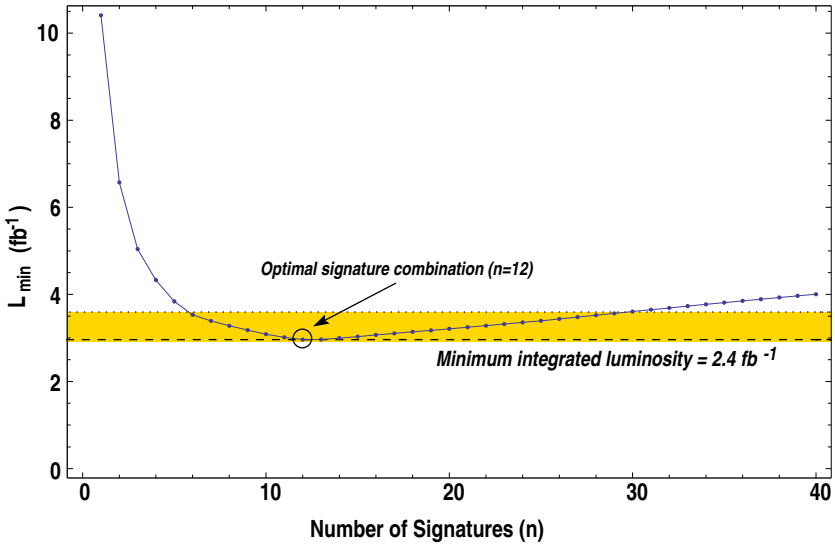

Figure 1. **An example of finding an "optimal" signature list.** By sequentially ordering the calculated $(L_{\min})_i$ values for any particular pair of models in ascending order, it is always possible to find the optimal set of signatures for that pair by applying (3.14). In this particular example the minimum value of $L_{\min}$ is found after combining just the first 12 signatures. After just the best six signatures we are already within 20% of the optimal value, as indicated by the shaded band.

20% higher than this minimal value then we need only $\mathcal{O}(5)$ signatures, typically.[4] This 20% range is indicated by the shaded band in figure 1. Of course this "optimal" set of signatures $\{S_i\}$ is only optimal for the specific pair of models A and B. We must repeat this optimization procedure on a large collection of model pairs and form a suitable average of the results in order to find a set of signatures $\{S_i\}$ that best approximates the truly optimal set over the widest possible set of model pairs $\{A, B\}$. The lists we will present at the end of this section represent the results of just such a procedure.

But before we present them, we must now address the issue of correlations. To be able to use the analytic results of our statistical presentation of the problem in section 3.2 we must be careful to only choose signatures from a list in which all the members are uncorrelated with one another. This immediately suggests a dilemma: once a signature is chosen, many others in the grand set will now be excluded for being correlated with the first. This complicates the process of optimization considerably — the task now becomes to perform the above optimization procedure over the largest possible list of *uncorrelated* (or at least minimally correlated) signatures. To find the correlation between any two signatures S_i and S_j it is sufficient to construct their correlation coefficient ρ_{ij}, given by

$$\rho_{ij} = \frac{\mathrm{cov}(i,j)}{\mathrm{var}(i)\mathrm{var}(j)} = \lim_{N\to\infty} \frac{\frac{1}{N}\sum_k \left[\bar{\sigma}_i^k - \sigma_i\right]\left[\bar{\sigma}_j^k - \sigma_j\right]}{\sqrt{\frac{1}{N}\sum_k \left[\bar{\sigma}_i^k - \sigma_i\right]^2}\sqrt{\frac{1}{N}\sum_k \left[\bar{\sigma}_j^k - \sigma_j\right]^2}}\,, \tag{3.15}$$

[4] It is interesting to compare this to the results of [6] in which the effective dimension of signature space was found to be also $\mathcal{O}(5)$ to $\mathcal{O}(10)$.

JHEP04(2009)114

Object	Minimum p_T	Minimum $\|\eta\|$
Photon	20 GeV	2.0
Electron	20 GeV	2.0
Muon	20 GeV	2.0
Tau	20 GeV	2.4
Jet	50 GeV	3.0

Table 2. **Initial cuts to keep an object in the event record**. After event reconstruction using the package PGS4 we apply additional cuts to the individual objects in the event record. Detector objects that fail to meet the above criteria are removed from the event record and do not enter our signature analysis. These cuts are applied to all analysis described in this paper.

where the $\bar{\sigma}^k$ represent the individual results obtained from each of the N cross section measurements, labeled by the index k.

In our analysis we estimated the entries in the 128×128 dimensional matrix of (3.15) in the following crude manner. We began with a simple MSSM model specified by a parameter set as in (3.1), with gaugino masses having the unified ratios of (1.2). We simulated this model $N = 2000$ times, each time with a different random number seed. The simulation involved generating $5\,\text{fb}^{-1}$ of events using PYTHIA 6.4, which were passed to the detector simulator PGS4. After simulating the detector response and object reconstruction the default level-one triggers included in the PGS4 detector simulation were applied. Further object-level cuts were then performed, as summarized in table 2. After these object-specific cuts we then applied an event-level cut on the surviving detector objects similar to those used in [6]. Specifically we required all events to have missing transverse energy $\not{E}_T > 150$ GeV, transverse sphericity $S_T > 0.1$, and $H_T > 600$ GeV (400 GeV for events with 2 or more leptons) where $H_T = \not{E}_T + \sum_{\text{Jets}} p_T^{\text{jet}}$. Once all cuts were applied the grand list of 128 signatures was then computed for each run, and from these signatures the covariance matrix in (3.15) was constructed. All histograms and counting signatures were constructed and analyzing using the ROOT-based analysis package Parvicursor [44].

Not surprisingly, many of the signatures considered in our grand list of 128 observables were highly correlated with one another. For example, the distribution of transverse momenta for the hardest jet in any event was correlated with the overall effective mass of the jets in the events (defined as the scalar sum of all jet p_T values: $M_{\text{eff}} = \sum_{\text{Jets}} p_T^{\text{jet}}$). Both were correlated with the distribution of H_T values for the events, and so forth. The consistency of our approach would then require that only a subset of these signatures can be included. One way to eliminate correlations is to partition the experimental data into mutually-exclusive subsets through some topological criteria such as the number of jets and/or leptons. For example, the distribution of H_T values in the set having any number of jets and zero leptons will be uncorrelated with the same signature in the set having any number of jets and at least one lepton. Our analysis indicated that this partitioning strategy has its limitations, however. The resolving power of any given signature tends to diminish as the set it is applied to is made ever more exclusive. This is in part due to the diminishing cross-section associated with the more exclusive final state (recall that

JHEP04(2009)114

our metric for evaluating signatures is proportional to the cross-section). It is also the case that the statistical error associated with extracting these cross-section values from the counts will grow as the number of events drops. We were thus led to consider a very simple two-fold partitioning of the data:

$$\begin{aligned} N_{\text{jets}} \leq 4 \text{ versus } N_{\text{jets}} \geq 5, \\ N_{\text{leptons}} = 0 \text{ versus } N_{\text{leptons}} \geq 1. \end{aligned} \tag{3.16}$$

This choice of data partitioning is reflected in the signature tables at the end of this section.

Within each if the four subsets it is still necessary to perform a correlation analysis and construct the matrix in (3.15). Let us for the moment imagine that we are willing to tolerate a correlation among signatures given by some value ϵ. Then the matrix of correlations in (3.15) can be converted into a matrix C_{ab} which defines the uncorrelated signatures by assigning the values

$$C_{ab} = \begin{cases} 1 \text{ if } \rho_{ab} \leq \epsilon \\ 0 \text{ if } \rho_{ab} > \epsilon \,. \end{cases} \tag{3.17}$$

The matrix C_{ab} is actually the adjacency matrix of a graph[5] and the problem of finding all the possible sets of uncorrelated signatures is equivalent to finding all the complete subgraphs (or 'clique') of that graph. A complete graph is a graph which has an edge between each vertex. In terms of our problem, this means a set of signatures having at most a correlation at the level of ϵ between any two of them. This is a well-known problem in combinatorics that becomes exponentially more difficult to solve as the number of signatures increases. For our purposes we will be working with relatively small sets of signatures which were pre-selected on the basis of their effectiveness for separating $\alpha = 0$ from non-zero values of this parameter. Then from these sets we will proceed to build the maximal subgraph for our choice of allowed correlation ϵ.

We constructed a large number of model families in the manner described in section 3.1, each involving the range $-0.5 \leq \alpha \leq 1.0$ for the parameter α in steps of $\Delta\alpha = 0.05$. For each point along these model lines we generated 100,000 events using `PYTHIA 6.4` and `PGS4`. To this we added an appropriately-weighted Standard Model background sample consisting of $5\,\text{fb}^{-1}$ each of $t/\bar{t}$ and $b/\bar{b}$ pair production, high-p_T QCD dijet production, single $W^{\pm}$ and Z-boson production, pair production of electroweak gauge bosons (W^+W^-, $W^{\pm}Z$ and ZZ), and Drell-Yan processes. To examine which of our 128 signatures would be effective in measuring the value of the parameter α we fixed "model A" to be the point on each of the model lines with $\alpha = 0$ and then treated each point along the line with $\alpha \neq 0$ as a candidate "model B." Clearly each model line we investigated — and each α value along that line — gave slightly different sets of maximally effective signatures. The lists we will present in tables 3, 4 and 5 represent an ensemble average over these model lines, restricted to a maximum correlation amount ϵ as described above.

[5] A graph is a set of vertices connected by edges. An element of an adjacency matrix of a graph is 1 if there is an edge between two vertices, 0 otherwise.

JHEP04(2009)114

	Description	Min Value	Max Value
1	$M_{\rm eff}^{\rm any} = \not{E}_T + \sum_{\rm all} p_T^{\rm all}$ [All events]	1250 GeV	End

Table 3. **Signature List A**. The effective mass formed from the transverse momenta of all objects in the event (including the missing transverse energy) was the single most effective signature of the 128 signatures we investigated. Since this "list" is a single item it was not necessary to partition the data in any way. For this distribution we integrate from the minimum value of 1250 GeV to the end of the distribution.

	Description	Min Value	Max Value
1	$M_{\rm eff}^{\rm jets}$ [0 leptons, ≥ 5 jets]	1100 GeV	End
2	$M_{\rm eff}^{\rm any}$ [0 leptons, ≤ 4 jets]	1450 GeV	End
3	$M_{\rm eff}^{\rm any}$ [≥ 1 leptons, ≤ 4 jets]	1550 GeV	End
4	p_T(Hardest Lepton) [≥ 1 lepton, ≥ 5 jets]	150 GeV	End
5	$M_{\rm inv}^{\rm jets}$ [0 leptons, ≤ 4 jets]	0 GeV	850 GeV

Table 4. **Signature List B**. The collection of our most effective observables, restricted to the case where the maximum correlation between any two of these signatures is 10%. Note that the jet-based effective mass variables would normally be highly-correlated if we had not partitioned the data according to (3.16). For these distributions we integrate from "Min Value" to "Max Value".

Let us begin with table 3, which gives the single most effective signature at separating models with different values of the parameter α. It is the effective mass formed from all objects in the event

$$M_{\rm eff}^{\rm any} = \not{E}_T + \sum_{\rm all} p_T^{\rm all}\,, \tag{3.18}$$

where we form the distribution from all events which pass our initial cuts. That this one signature would be the most powerful is not a surprise given the way we have set up the problem. It is the most inclusive possible signature one can imagine (apart from the overall event rate itself) and therefore has the largest overall cross-section. Furthermore, the variable in (3.18) is sensitive to the mass differences between the gluino mass and the lighter electroweak gauginos — precisely the quantity that is governed by the parameter α. Yet as we will see in section 4 this one signature can often fail to be effective at all in certain circumstances, resulting in a rather large required $L_{\rm min}$ to be able to separate $\alpha = 0$ from non-vanishing cases. In addition it is built from precisely the detector objects that suffer the most from experimental uncertainty. This suggests a larger and more varied set of signatures would be preferable.

We next consider the five signatures in table 4. These signatures were chosen by taking our most effective observables and restricting ourselves to that set for which $\epsilon = 10\%$. We again see the totally inclusive effective mass variable of (3.18) as well as the more traditional effective mass variable, $M_{\rm eff}^{\rm jets}$, defined via (3.18) but with the scalar sum of p_T values now running over the jets only. We now include the p_T of the hardest lepton in events with at least one lepton and five or more jets, as well as the invariant mass $M_{\rm inv}^{\rm jets}$ of

JHEP04(2009)114

	Description	Min Value	Max Value
	Counting Signatures		
1	N_ℓ [≥ 1 leptons, ≤ 4 jets]		
2	$N_{\ell^+\ell^-}$ [$M_{\rm inv}^{\ell^+\ell^-} = M_Z \pm 5$ GeV]		
3	N_B [≥ 2 B-jets]		
	[0 leptons, ≤ 4 jets]		
4	$M_{\rm eff}^{\rm any}$	1000 GeV	End
5	$M_{\rm inv}^{\rm jets}$	750 GeV	End
6	$\not{E}_T$	500 GeV	End
	[0 leptons, ≥ 5 jets]		
7	$M_{\rm eff}^{\rm any}$	1250 GeV	3500 GeV
8	$r_{\rm jet}$ [3 jets > 200 GeV]	0.25	1.0
9	p_T(4th Hardest Jet)	125 GeV	End
10	$\not{E}_T/M_{\rm eff}^{\rm any}$	0.0	0.25
	[≥ 1 leptons, ≥ 5 jets]		
11	$\not{E}_T/M_{\rm eff}^{\rm any}$	0.0	0.25
12	p_T(Hardest Lepton)	150 GeV	End
13	p_T(4th Hardest Jet)	125 GeV	End
14	$\not{E}_T + M_{\rm eff}^{\rm jets}$	1250 GeV	End

Table 5. **Signature List C**. In this collection of signatures we have allowed the maximum correlation between any two signatures to be as high as 30%. Note that some of the signatures are normalized signatures, (#8, #10 and #11), while the first three are truly counting signatures. A description of each of these observables is given in the text. For all distributions we integrate from "Min Value" to "Max Value".

the jets in events with zero leptons and 4 or less jets. The various jet-based effective mass variables would normally be highly correlated with one another if we were not forming them from disjoint partitions of the overall data set. The favoring of jet-based observables to those based on leptons is again largely due to the fact that jet-based signatures will have larger effective cross-sections for reasonable values of the SUSY parameters in (3.1) than leptonic signatures. The best signatures are those which track the narrowing gap between the gluino mass and the electroweak gauginos and the narrowing gap between the lightest chargino/second-lightest neutralino mass and the LSP mass. In this case the first leptonic signature to appear — the transverse momentum of the leading lepton in events with at least one lepton — is an example of just such a signature.

Finally, let us consider the larger ensemble of signatures in table 5. In this final set we have relaxed our concern over the issue of correlated signatures, allowing as much as 30% correlation between any two signatures in the list. This allows for a larger number as well as a wider variety of observables to be included. As we will see in section 4 this can be very important in some cases in which the supersymmetric model has unusual properties, or in cases where the two α values being considered give rise to different mass orderings (or hierarchies) in the superpartner spectrum. In displaying the signatures in table 5 we

JHEP04(2009)114

find it convenient to group them according to the partition of the data being considered. Note that the counting signatures are taken over the entire data set.

The first counting signature is simply the total size of the partition from (3.16) in which the events have at least one lepton and 4 or less jets. This was the only observable taken on this data set that made our list of the most effective observables. The next two signatures are related to "spoiler" modes for the trilepton signal. Note that the trilepton signal itself did *not* make the list: this is a wonderful discovery mode for supersymmetry, but the event rates between a model with $\alpha = 0$ and one with non-vanishing α were always very similar (and low). This made the trilepton counting signature ineffective at distinguishing between models. By contrast, counting the number of b-jet pairs (a proxy for counting on-shell Higgs bosons) or the number of opposite-sign electron or muon pairs whose invariant mass was within 5 GeV of the Z-mass (a proxy for counting on-shell Z-bosons) *were* excellent signatures for separating models from time to time. This was especially true when the two models in question had very different values of α such that the mass differences between $\widetilde{N}_2$ and $\widetilde{N}_1$ were quite different in the two cases. We will give specific examples of such outcomes in section 4.

The following three sections of table 5 involve some of the same types of observables as in the previous tables, with a few notable changes and surprises. First note that several of the observables in table 5 involve some sort of normalization. In particular numbers 8, 10 and 11. Our estimate of the correlations among signatures found that the fluctuations of these normalized signatures tended to be less correlated with other observables for that partition than the un-normalized quantities. However, normalizing signatures in this way also tended to reduce their ability to distinguish models. Signature #8 is defined as the following ratio

$$r_{\rm jet} \equiv \frac{p_T^{\rm jet3} + p_T^{\rm jet4}}{p_T^{\rm jet1} + p_T^{\rm jet2}} \tag{3.19}$$

where $p_T^{\rm jet\,i}$ is the transverse momentum of the i-th hardest jet in the event. For this signature we require that there be at least three jets with $p_T > 200$ GeV. This signature, like the p_T of the hardest lepton or the p_T of the 4th hardest jet, was effective at capturing the increasing softness of the products of cascade decays as the value of α was increased away from $\alpha = 0$.

Let us note that Lists A, B and C are not mutually disjoint. For example, signatures 4, 5 and 12 of table 5 also appear in table 4. The signature mix is determined by attempting to minimize $L_{\rm min}$ via the formula in (3.14) while attempting to keep the correlations between any pair of signatures below the targets set above in the text. As mentioned earlier, larger lists are not always better — the more signatures one adds, the larger the likelihood that some pair will be correlated with one another to an unsatisfactory amount. Furthermore, when signatures are added which are only occasionally useful, the resolving power of the ensemble can actually be degraded since the statistical threshold defined by $\lambda_{\rm min}$ in table 11 grows with the number of signatures.

We will see some examples of this perverse effect in the next section in which we will examine the effectiveness of these three lists. We will do this first against our benchmark

JHEP04(2009)114

models from section 2 and then against a large ensemble of random MSSM model lines. Before doing so let us note that by fixing a particular set of n signatures in every instance — and indeed, with the fixed integration ranges indicated in the tables — we are very likely to often be far from the *optimal* signature mix and integration ranges. That is, we should not expect to achieve the absolute $L_{\rm min}$ value of figure 1 for any particular pair or points along a model line. If we have chosen our signature list well, however, then we can hope that the result of adding the contributions of all n signatures using (3.14) will be close to the optimal $L_{\rm min}$ value over a large array of model pairs.

4 Analysis results

In this section we will examine how well our signature lists in tables 3, 4 and 5 perform in measuring the value of the parameter α which appears in (1.1). Recall that our specific goal is to distinguish between a model with $\alpha = 0$ and another with *all other soft terms held equal*, but with $\alpha \neq 0$. We would like to do this with the least amount of data (or integrated luminosity) as possible for the smallest values of α possible. We will first demonstrate how the lists perform on our benchmark cases before turning to an analysis of their performance on a large ensemble of randomly-generated supersymmetric models.

4.1 Benchmark models analysis

We begin with the theory-motivated benchmark models briefly mentioned at the end of section 2 and discussed at length in the appendix. The input values for the soft supersymmetry-breaking parameters are listed in table 1 at the very end of section 2. To remind the reader, model A is an example of a heterotic string compactification with Kähler stabilization of the dilaton while model B is an example of a Type IIB string model with flux compactification. Each of these examples predicts a particular value of α as a function of other parameters in the theory; specifically, model A predicts $\alpha \simeq 0.3$, while model B predicts $\alpha \simeq 1$. Further details can be found in the appendix (and references therein), but these details are not relevant for our purposes in this section.

The input values of table 1 were evolved from the input scale $\Lambda_{\rm UV} = 2 \times 10^{16}$ GeV to the electroweak scale of 1 TeV by solving the renormalization group equations. For this we use the computer package `SuSpect` [45], utilizing two-loop running for all parameters *except* for the gaugino masses. For these we use one-loop RGEs only in order to maintain the parametrization for the gaugino soft parameters in terms of α given by (1.1). Once run to the low scale the physical spectra and mixings of the models were computed by `SuSpect`. The result of this process for our two benchmark models is given in table 6.

From here we performed a simulation using the combined package of `PYTHIA` + `PGS4` as described in section 3.3. For each of these two models a model-line was generated by varying the parameter α from $\alpha = 0$ to $\alpha = 1$, in increments of 0.05, while keeping all other soft parameters fixed. Along these model lines the gluino soft mass M_3 was held constant to set the overall scale, and the two parameters M_1 and M_2 were varied according to the ratios in (1.1). For each point 500,000 events were generated using the L1 trigger options in `PGS4`. After applying further initial cuts as described in section 3.3 the signatures associated with

JHEP04(2009)114

Parameter	Point A	Point B		Parameter	Point A	Point B
$m_{\widetilde{N}_1}$	85.5	338.7		$m_{\tilde{t}_1}$	844.7	379.9
$m_{\widetilde{N}_2}$	147.9	440.2		$m_{\tilde{t}_2}$	1232	739.1
$m_{\widetilde{N}_3}$	485.3	622.8		$m_{\tilde{c}_L}$, $m_{\tilde{u}_L}$	1518	811.7
$m_{\widetilde{N}_4}$	494.0	634.3		$m_{\tilde{c}_R}$, $m_{\tilde{u}_R}$	1520	793.3
$m_{\widetilde{C}_1^\pm}$	147.7	440.1		$m_{\tilde{b}_1}$	1224	676.8
$m_{\widetilde{C}_2^\pm}$	494.9	635.0		$m_{\tilde{b}_2}$	1507	782.4
$m_{\tilde{g}}$	510.0	818.0		$m_{\tilde{s}_L}$, $m_{\tilde{d}_L}$	1520	815.4
μ	476.1	625.2		$m_{\tilde{s}_R}$, $m_{\tilde{d}_R}$	1520	793.5
m_h	115.2	119.5		$m_{\tilde{\tau}_1}$	1487	500.4
m_A	1557	807.4		$m_{\tilde{\tau}_2}$	1495	540.4
m_{H^0}	1557	806.8		$m_{\tilde{\mu}_L}$, $m_{\tilde{e}_L}$	1500	545.1
$m_{H^\pm}$	1559	811.1		$m_{\tilde{\mu}_R}$, $m_{\tilde{e}_R}$	1501	514.6

Table 6. **Low energy physical masses for benchmark points**. Low energy physical masses (in units of GeV) are given at the scale 1 TeV. All points are taken to have $\mu > 0$. The actual value of $\tan\beta$ is fixed in the electroweak symmetry-breaking conditions. Model A represents a mirage model with $\alpha = 0.3$ while Model B has $\alpha = 1$.

each of the three lists in tables 3, 4 and 5 were constructed. We then used the criterion for distinguishability described in section 3.2 to determine the minimum luminosity $L_{\rm min}$ needed to separate $\alpha = 0$ from all other points along the line.

The results of this analysis are presented in the top panels of figure 2. The plot on the left corresponds to benchmark model A while the one on the right corresponds to benchmark model B. The vertical axis shows the minimum luminosity needed to separate a given $\alpha \neq 0$ scenario from the unified case of $\alpha = 0$. The three shaded regions represent the three model lists we used to analyze the data. At the lower edge of each region is the value of $L_{\rm min}$ as calculated using the relations in (3.13) and (3.14). The upper edge of each region represents an estimate of the 1 sigma upper bound on the calculated value of $L_{\rm min}$ caused by statistical fluctuations (i.e. the fact that the cross-sections extracted from the data or simulation are not the true cross-sections for each signature). The lower panels in figure 2 represent the same analysis, but now each of the two models are compared to their predicted values: $\alpha = 0.3$ for model A and $\alpha = 1.0$ for model B. With the exception of the straw-man List A in the case of benchmark model A, all the lists do an adequate job of distinguishing points along these alpha-lines with moderate amounts of integrated luminosity. Naturally, as the two points being compared approach one another the signature difference between them become smaller and the needed $L_{\rm min}$ increases. It is instructive to consider the case of model A to understand why some approaches to extracting the parameter α succeed and others fail.

Model A has nearly universal scalar masses at a rather high scale of approximately 1.5 TeV, yet the light gluino makes this the model with the higher overall cross-section. All supersymmetric observables in this benchmark model are therefore dominated by gluino pair production and their eventual cascade decays through highly off-shell squarks. In

JHEP04(2009)114

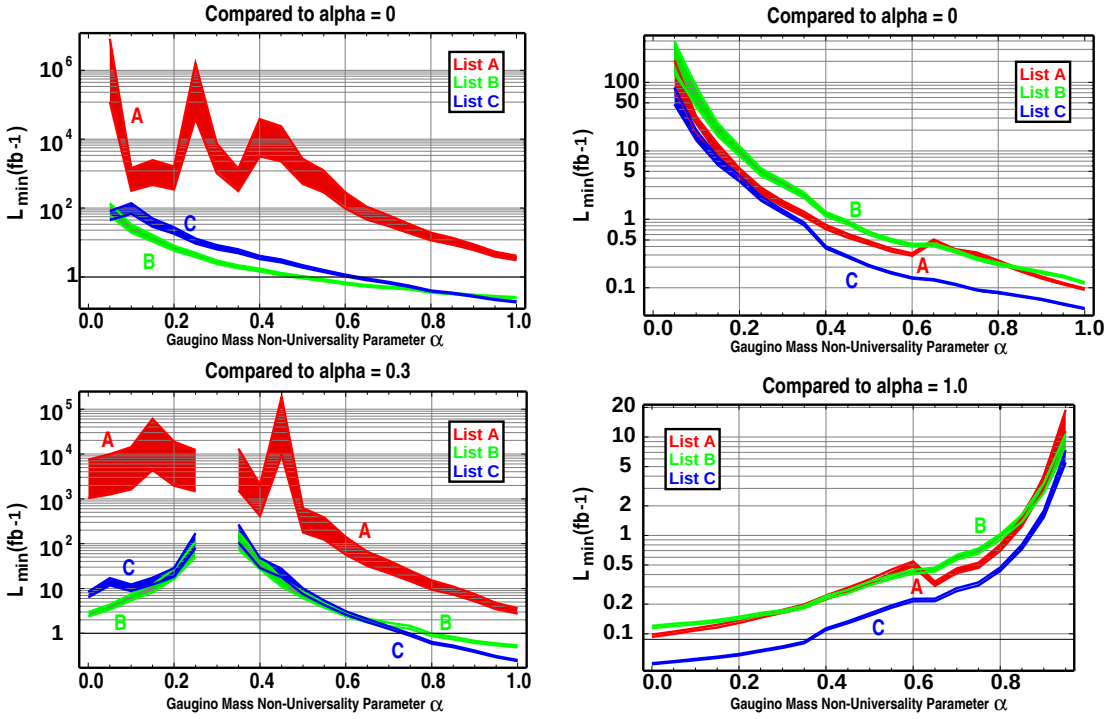

Figure 2. $L_{\rm min}$ **as a function of** α **for the two benchmark models.** The three shaded regions correspond to the three signature lists as indicated by the legend. The lower bound of each shaded region indicates the minimum integrated luminosity $L_{\rm min}$ needed to separate the model with the specified α from $\alpha = 0$ (top panels) or the predicted value of α (lower panels). The upper bound of the shaded region represents an estimate of the 1 sigma upper bound on the calculated value of $L_{\rm min}$ caused by statistical fluctuations.

the analysis the gluino mass is kept constant along an alpha-line, so the cross-section for the dominant process $gg \to \tilde{g}\tilde{g}$ is fixed at $\sigma(gg \to \tilde{g}\tilde{g}) = 13.4\,\text{pb}$ for this alpha-line. Any signatures related to this variable will depend on α only via the change in the gluino branching fractions, which are nearly constant as a function of the parameter α.[6] Blunt signatures like the total $M_{\rm eff}$ variable of (3.18) indicate roughly the total production cross-section and crude mass scale of the superpartner being predominantly produced. This is an example in which the most inclusive possible observable is simply too inclusive to detect the change in gaugino mass ratios. For this one must consider processes that produce electroweak gauginos, which are subdominant by as much as a factor of ten in the case of benchmark model A.

Further compounding the problems for the inclusive signature of List A is the fact that the count rate for this particular final state is varying only very slowly with α. Despite the fact that this count rate can be quite large in this model, the resulting value of $L_{\rm min}$ is high because the ΔS_{AB} value for this particular signature is very near zero. As a result,

[6]Only the highly suppressed three-body decay $\tilde{g} \to \tilde{C}_1 q\bar{q}'$ with q and $\bar{q}'$ representing third-generation quarks shows any significant dependence on the value of the parameter α for this benchmark model.

JHEP04(2009)114

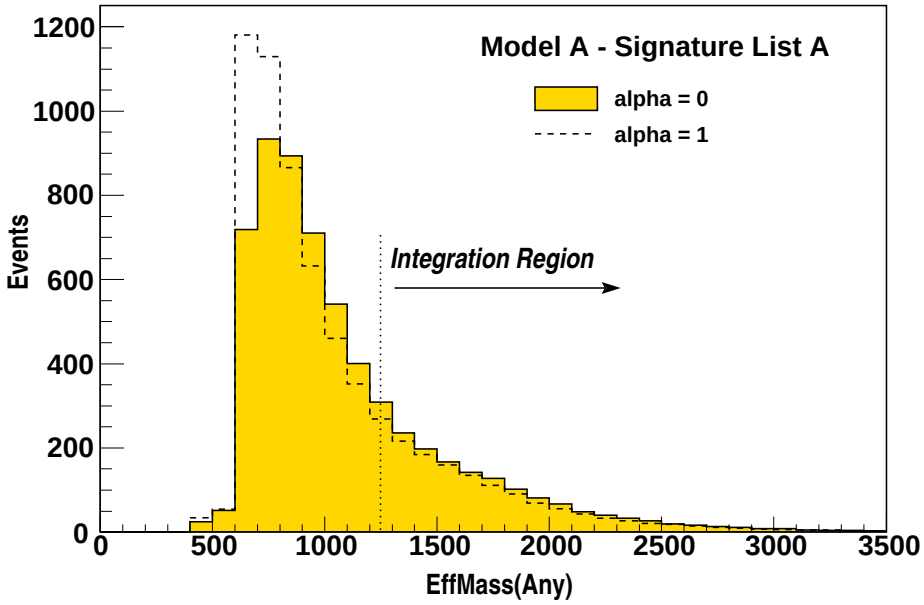

Figure 3. Distribution of the variable $M_{\rm eff}^{\rm any}$ from signature List A for benchmark model A. Solid filled histogram is the case for $\alpha = 0$, dotted histogram is the case for $\alpha = 1$. The lower bound for the integration region is indicated by the dotted line at 1250 GeV. The sharp lower bound in the distribution is an artefact of the event-level cuts imposed on the data as described in section 3.3. In this case the failure of List A to separate the two cases is apparent: the difference between the two histograms is negligible above the value $M_{\rm eff}^{\rm any} = 1250$ GeV. The resolving power would improve dramatically if this lower bound was relaxed to $M_{\rm eff}^{\rm any} = 500$ GeV, as demonstrated in figure 4.

small statistical fluctuations in the data or the simulation result in large fluctuations in the resulting value of $L_{\rm min}$ needed to truly separate different values of the parameter α. This reflects itself in both the width of the shaded region in the left panels of figure 2 and in the volatility of the extracted value itself. In figure 3 we plot the distribution of the List A variable (3.18) in benchmark model A for the case of $\alpha = 0$ (solid line) and $\alpha = 1$ (dashed line). Above our integration cut of 1250 GeV there is very little difference between the distributions, even for this extreme case. However, it is clear that some discrimination power is available had we chosen a different lower bound for integration. When the lower bound on this particular variable is relaxed to 500 GeV the inclusive $M_{\rm eff}$ variable becomes competitive with the other signature lists, as shown in figure 4.

Benchmark model A therefore provides us with an example where the procedure of optimizing the signature list over a wide ensemble of models has produced a prescription that is most definitely *not* optimal for this particular case. Once a particular model framework is established it will of course be possible to tailor analysis techniques to optimize the statistical power of any given signature. But for our quasi-model-independent analysis we must forgo optimization in favor of generality. Nevertheless, we gain resolving power by simply expanding the list of signatures to include those which are more sensitive to the

JHEP04(2009)114

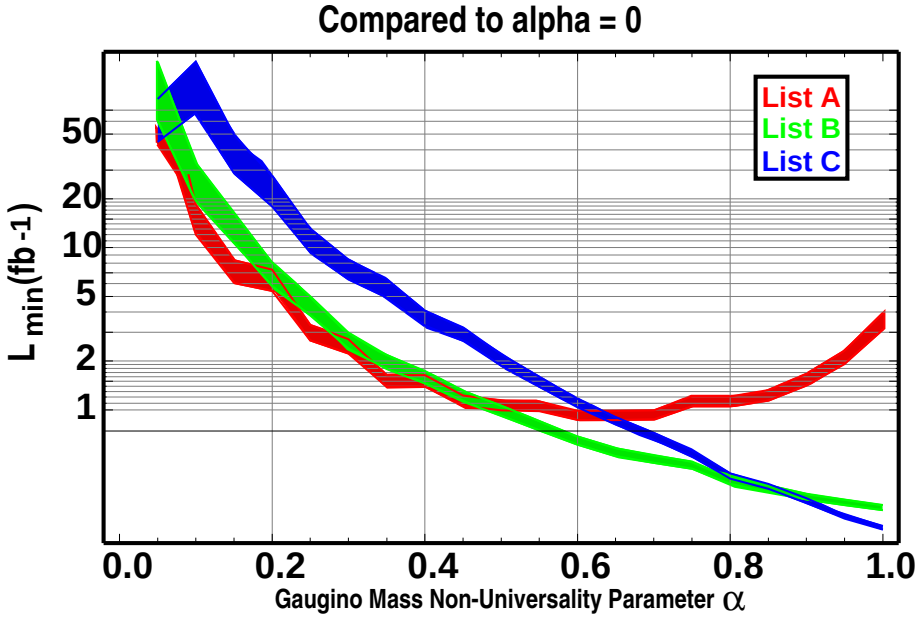

Figure 4. $L_{\rm min}$ **as a function of** α **for benchmark model A with relaxed lower bound on** $M_{\rm eff}^{\rm any}$**.** The three shaded regions correspond to the three signature lists as in the upper left panel of figure 2. In this case the lower bound of the integration range for the single observable of List A has been relaxed to 500 GeV.

changes in the lower-mass electroweak gaugino spectrum. Returning to the left panels of figure 2 it is clear that Lists B and C do far better at measuring the parameter α than the single $M_{\rm eff}$ variable alone. For example, the jet invariant mass variables in both lists, as well as the normalized $\not{E}_T$ signatures and $p_T(\text{Jet}_4)$ observable of List C are much more sensitive to changes in α for this benchmark model than the observable in (3.18).

But note the *reduction* in resolving power that occurs when we choose the largest signature list. As discussed in section 3.3, it is clear that the largest possible signature list is not always the most effective at separating two theories. In this particular example many of the additional observables in List C are not at all helpful in separating different α values — particularly the counting variables for which the total rates are low and the differences across the alpha-line are small. These additional variables were designed to be most effective when the mass hierarchies in the superpartner spectrum change as the value of α is modified, so that dramatic changes in production rates and/or branching ratios occur. Such threshold effects do not occur over the α range probed in benchmark model A, but do in fact occur for benchmark model B. This is clearly evident in the right panels of figure 2, where additional resolving power is obtained when using the expanded signature List C.

We note that the single inclusive variable of (3.18) is much more effective in benchmark model B in part because the production cross-sections for all SU(3)-charged superpartners are roughly equal in magnitude. The inclusive $M_{\rm eff}$ variable no longer tracks the mass and decay products of a single heavy state so variations with the parameter α are now more

JHEP04(2009)114

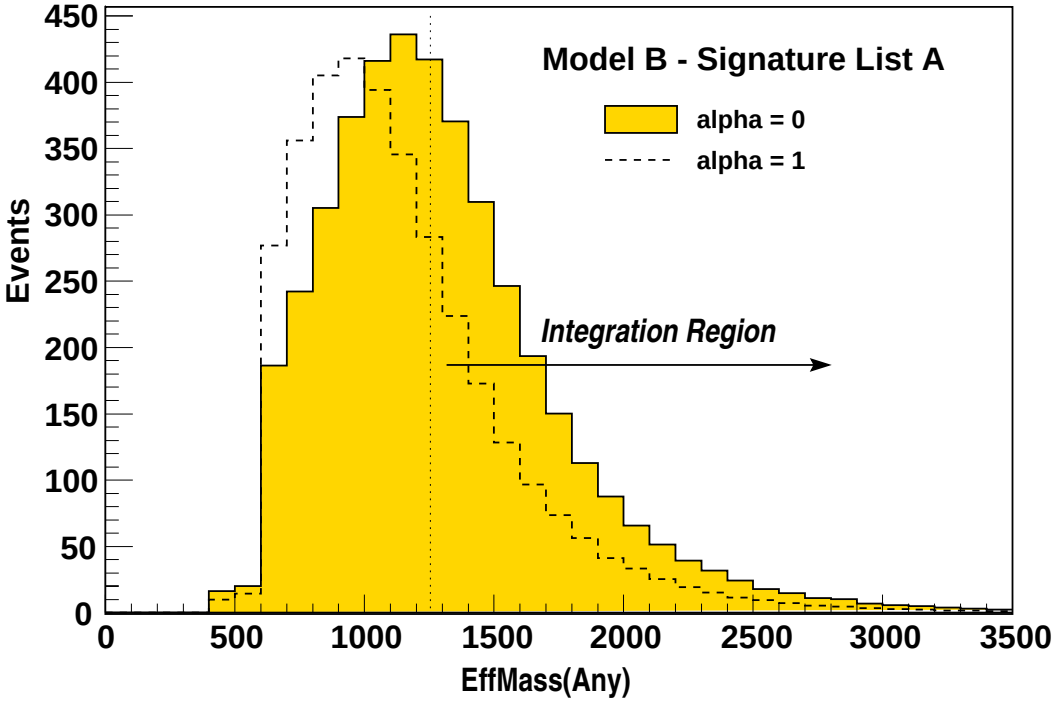

Figure 5. Distribution of the variable $M_{\rm eff}^{\rm any}$ from signature List A for benchmark model B. Solid filled histogram is the case for $\alpha = 0$, dotted histogram is the case for $\alpha = 1$. The lower bound for the integration region is indicated by the dotted line at 1250 GeV. The sharp lower bound in the distribution is an artefact of the event-level cuts imposed on the data as described in section 3.3.

prominent. This is shown in figure 5, which should be compared to the case of model A in figure 3. Note that the total area under the two curves in figure 5 is nearly identical, highlighting the need to choose a wise value of the lower bound on the integration region to achieve a high degree of differentiation. Model B is similar to the randomly-generated models we used to design our signature lists and thus the chosen value of 1250 GeV for this particular observable is close to what would be the optimal choice for this particular model comparison.

Despite the lower overall cross-section for the supersymmetric signal in benchmark model B, the three signature lists succeed in distinguishing the case $\alpha = 0$ from non-vanishing cases with far less integrated luminosity. In large part this is due to the richness of the particle spectrum for this model. The superpartner masses given in table 6 are for the case $\alpha = 1$. As α approaches zero the masses of the lighter neutralinos and lightest chargino fall relative to that of the gluinos and squarks (which remain constant). Along this alpha-line several important thresholds are crossed, resulting in dramatic changes in the relevant branching fractions for the heavier states. The mix of signatures in List B and List C that contribute most strongly to the resolving power of the overall list changes as we move along the alpha-line. For example, consider the $(R_{AB})_i$ values of (3.10) for the five signatures of List B. We plot these values in figure 6 for model A corresponding to $\alpha = 0$ and model B corresponding to the indicated value of $\alpha \neq 0$.

JHEP04(2009)114

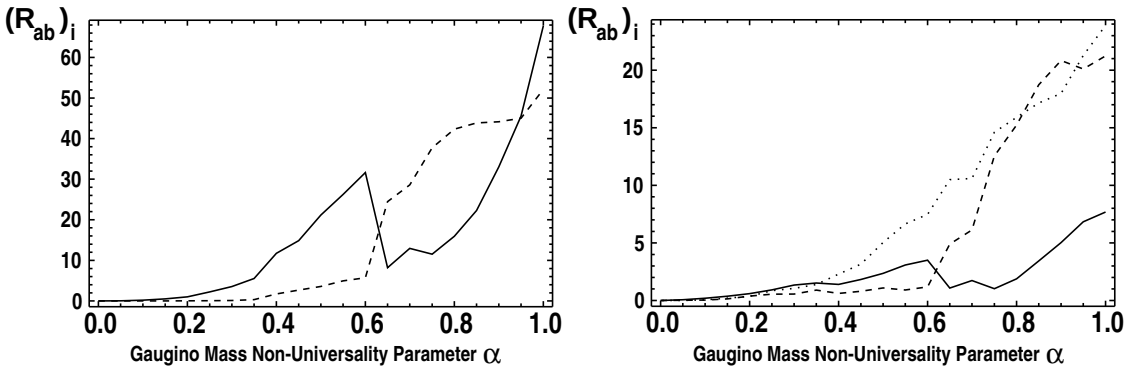

Figure 6. **Values of $(R_{AB})_i$ for the five signatures of List B as a function of α for benchmark model B.** The ability of each individual signature from List B to resolve the case $\alpha = 0$ from the indicated value of α is given by the height of the curve $(R_{AB})_i$ in the above plots. In the left panel we display signature 1 (solid curve) and signature 5 (dashed curve). In the right panel we display signature 2 (solid curve), signature 3 (dashed curve) and signature 4 (dotted curve).

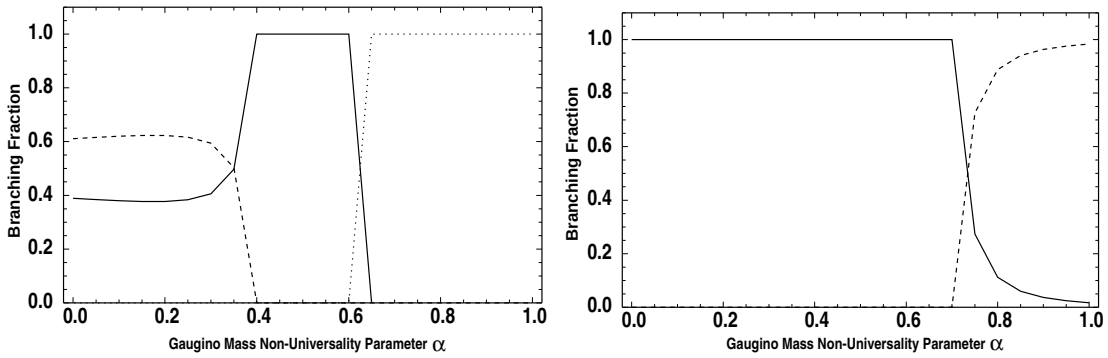

Figure 7. **Branching fractions for principal decay modes of lightest stop (left panel) and lightest chargino (right panel) as a function of α for benchmark model B.** In the left panel the decay modes are $\tilde{t}_1 \to \tilde{N}_1 t$ (dashed curve), $\tilde{t}_1 \to \tilde{C}_1 b$ (solid curve), and $\tilde{t}_1 \to \tilde{N}_1 c$ (dashed curve). In the right panel the decay modes are $\tilde{C}_1 \to \tilde{N}_1 W$ (solid curve) and $\tilde{C}_1 \to \tilde{t}_1 \bar{b}$ (dashed curve).

To understand these curves, we first note that the dominant SUSY production processes in benchmark model B are the pair production of stops and associated production of light squarks with a gluino. The branching fraction for three of the more important decay modes of the stop are plotted versus the parameter α in the left panel of figure 7. For values of $\alpha \lesssim 0.35$, when both the chargino $\tilde{C}_1$ and the LSP $\tilde{N}_1$ are sufficiently light, the direct two-body decay into the LSP and a top quark is dominant. About 50% of the time the W-bosons from the top decays on both sides of the events will decay hadronically and the event will be captured by the first observable in List B. For the intermediate region $0.35 \lesssim \alpha \lesssim 0.6$ the stop decays predominantly via $\tilde{t}_1 \to \tilde{C}_1 b$ and the final state topology is determined by the subsequent decay of the chargino. The branching fractions for the

JHEP04(2009)114

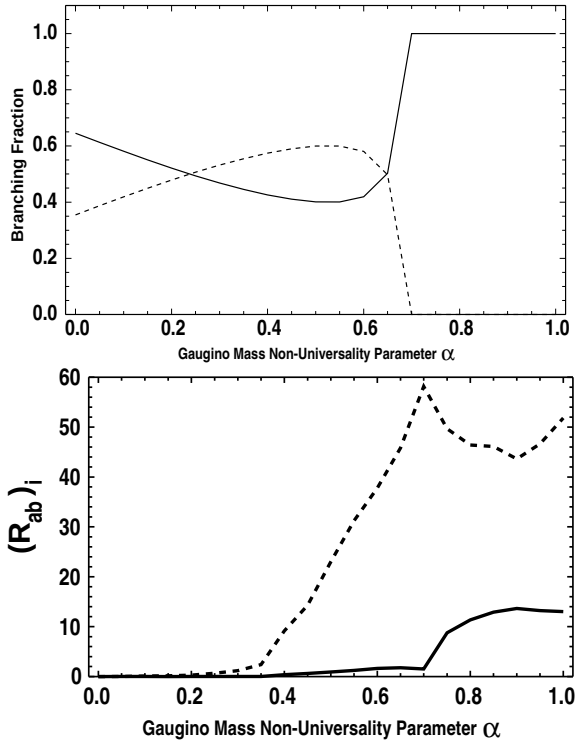

Figure 8. **Branching fraction for next-to-lightest neutralino (left) and $(R_{AB})_i$ values for key counting signatures from List C (right).** The branching fraction of the next-to-lightest neutralino $\tilde{N}_2$ for benchmark model B is plotted as a function of α in the left panel. The decay modes are $\tilde{N}_2 \to \tilde{N}_1\, h$ (dashed curve) and $\tilde{N}_2 \to \tilde{N}_1\, Z$ (solid curve). In the right panel the $(R_{AB})_i$ values for the inclusive leptonic counting signature (signature 1 — solid curve) and the inclusive B-jet counting signature (signature 3 — dashed curve) are plotted as function of α.

primary decay channels of the chargino $\tilde{C}_1$ are given in the right panel of figure 7. In this intermediate α region the chargino is decaying primarily to a W-boson, populating all of the signatures in List B.

For larger values of $\alpha \gtrsim 0.6$ the chargino $\tilde{C}_1$ and the LSP $\tilde{N}_1$ are now massive enough that the only decay channel available for the stops is the process $\tilde{t}_1 \to \tilde{N}_1 c$, producing $\not{E}_T$ and two jets only. These events are captured by the second and (especially) fifth observables in List B, as evidenced by their rapid growth in significance. For $\alpha \gtrsim 0.7$ charginos that are directly produced (or produced through cascade decays of heavier squarks) will now decay *into* stops via $\tilde{C}_1 \to \tilde{t}_1 b \to \tilde{N}_1 cb$. This boosts the resolving power of the signatures with lepton vetoes relative to the other signatures in List B.

Similar arguments explain the behavior of the expanded list of observables in List C. Here we will only take a moment to mention the counting signatures which make their first appearance in our analysis. Generally speaking, counting signatures are sensitive only to the total cross-section for the final state being counted. Changes in the p_T of Standard Model particles produced in cascades are washed out, making them less useful for comparing different gaugino mass hierarchies. Counting signatures are therefore only

JHEP04(2009)114

Input Parameter Range	Variation
$400 \text{ GeV} \geq M_3 \geq 800 \text{ GeV}$	5 steps
$400 \text{ GeV} \geq \mu \geq 1000 \text{ GeV}$	5 steps
$300 \text{ GeV} \geq (m_{\tilde{e}_{L,R}}, m_{\tilde{\tau}_{L,R}}) \geq 700 \text{ GeV}$	5 steps
$500 \text{ GeV} \geq (m_{\tilde{Q}_L}, m_{\tilde{q}_L}, m_{\tilde{t}_{L,R}}, m_{\tilde{b}L,R}) \geq 1000 \text{ GeV}$	5 steps
$\tan\beta = 10$	Fixed
$m_A = 1000 \text{ GeV}$	Fixed
$A_\tau,\ A_t,\ A_b,\ A_e,\ A_u,\ A_d = 0$	Fixed

Table 7. **MSSM soft parameters ranges and variation steps used to generate controlled sample.** These values are given at the electroweak scale. For each choice of MSSM input, the gaugino unification parameter α was varied in four steps, from $\alpha = 0$ to $\alpha = 1.0$

effective when the two α values being compared correspond to different decay patterns altogether. This happens in several instances in benchmark model B, as we indicated above. The counting signatures in List C are specifically designed to consider changes in the decay table for the next-to-lightest neutralino $\tilde{N}_2$ — particularly the appearance of the so-called "spoiler" modes for the classic trilepton signal. In the left panel of figure 8 the primary decay modes of the next-to-lightest neutralino $\tilde{N}_2$ are given. We observe that both of the on-shell decays $\tilde{N}_2 \to \tilde{N}_1 h$ and $\tilde{N}_2 \to \tilde{N}_1 Z$ are available for this state when $\alpha \lesssim 0.7$, with the Higgs mode peaking around $\alpha \simeq 0.6$ before becoming kinematically inaccessible. This changeover is reflected in the R_i values for the leptonic counting signature and the B-jet counting signature of List C, as shown in the right panel of figure 8. Note that the light stop in benchmark model B makes this a very B-jet rich point. In fact, this particular counting signature is one of the most effective observables in List C along the alpha-line for this point.

4.2 Analysis of a large set of model variations

We next examine the efficacy of our method by testing it on a large sample of varying model points. We will do this in two steps: first on a controlled sample of models and subsequently on a random collection of model lines. Ranges for the MSSM input parameters and variation steps used for our controlled sample are given in table 7. Only M_3, $m_{\tilde{l}}$, $m_{\tilde{q}}$, and μ were allowed to vary across 5 uniform steps. All other soft parameters were held constant. The gaugino universality parameter α was also varied in 4 steps from $\alpha = 0$, to 0.33, 0.66, and 1.0. These choices discretize the range of parameter space into 2500 individual model points. Note that the parameters of table 7 are given at the low-energy electroweak scale. We emphasize the fact that in this first step we have chosen to sample the parameter space on a discrete grid rather than sampling it randomly. While a truly random sampling is necessary for ultimately testing our method, we here wish to study the performance of our signature sets as key parameters are varied. Our discrete grid is designed to keep the overall supersymmetric production rate roughly fixed, allowing for a more straightforward comparison of $L_{\min}$ values. In order to minimize computation time

JHEP04(2009)114

Largest Production Channel				
Mode	$\alpha = 0$	$\alpha = 0.33$	$\alpha = 0.66$	$\alpha = 1.0$
$gg \to \tilde{g}\tilde{g}$	44.6%	45.2%	42.9%	44.8%
$fg \to \tilde{q}_R\tilde{g}$	31.1%	30.2%	33.1%	35.7%
$fg \to \tilde{q}_L\tilde{g}$	24.3%	25.5%	23.9%	19.4%
Second Largest Production Channel				
Mode	$\alpha = 0$	$\alpha = 0.33$	$\alpha = 0.66$	$\alpha = 1.0$
$gg \to \tilde{g}\tilde{g}$	2.7%	2.1%	2.8%	1.4%
$fg \to \tilde{q}_R\tilde{g}$	42.0%	48.8%	47.5%	45.2%
$fg \to \tilde{q}_L\tilde{g}$	42.0%	47.1%	49.6%	53.3%
$f_i f_j \to \tilde{\chi}_2^0\tilde{\chi}_1^\pm$	13.2%	1.9%	-	-

Table 8. **Dominant production modes across all model variations**. At a given α choice, the upper table indicates the percentage of models for which these modes had the largest cross section, while the lower table indicates the percentage for which the modes had the second-largest cross-section. All models exhibit predominantly gluino pair production, or gluino-quark associated production. A small fraction of $\alpha = 0$ models exhibit neutralino-chargino pair production. This mode 'switches off' as α is increased from zero, as the gaugino masses increase.

we chose a coarse grid spacing. While such a coarse grid cannot fully represent all model configurations possible with our parameter space, our choice of grid spacing sufficiently samples many of the distinct, phenomenologically interesting mass hierarchies possible in the spectrum, each of which can have rather different signatures. A finer spacing would result in many models with relatively little spectral variation, and no difference in spectral hierarchy, requiring additional computation time but yet providing no dramatic change in signature behavior. Our goal in studying this set is simply to show how our signatures lists perform as the underlying model is changed. Our final analysis of a truly random collection of models will appear at the end of this subsection.

Simulated data for the model points was generated with the following procedure. For each model, the `SuSpect` partner code `SusyHIT` [46] was used to compute the low-scale spectrum from the input MSSM soft terms. No renormalization group evolution was necessary because the input parameters were given at the electroweak scale. As before `PYTHIA` + `PGS4` was used to simulate the detector response for each point. A check was performed to ensure that each model point had a neutralino LSP, and also that each $\alpha \geq 0$ model point simulated had an associated $\alpha = 0$ counterpart, so that the minimum luminosity required to distinguish between the two models, $L_{\min}$, could be computed. Only models satisfying these requirements were retained for analysis. Exactly 1449 model pairs ($\alpha = 0$ and $\alpha \neq 0$) were retained after applying this selection procedure.

Table 8 gives the dominant production modes across the entire set of model variations. The upper table indicates the mode and percentage of models, for a given α choice, that occur with the largest cross-section. The lower table gives the same information for the modes that occur with the second-largest cross-section. The majority of models exhibit

JHEP04(2009)114

squark-gluino associated production, or gluino pair production as the dominant production mechanism. Approximately 13% of $\alpha = 0$ models, and about 2% of $\alpha = 0.33$ models have neutralino-chargino production as the second most dominant mode.

The particle decay behavior varies throughout the range of model simulations. However, gluino decays are largely insensitive to changes in α. For the case $\alpha = 0$, approximately 68% of models have $\tilde{g} \to \tilde{\chi}_1^{\pm} + \bar{q}q'$ as the primary decay channel (the channel having the largest branching fraction), while 31% of models have instead $\tilde{g} \to \tilde{b}_1 + b$ as the primary channel. The $\alpha = 0.33$ and 0.66 models exhibit similar ratios. The $\alpha = 1.0$ models show a slight variation, with the distribution shifting to 70% and ∼30% respectively. For all α values, approximately 68% of model variations also exhibit $\tilde{g} \to \tilde{\chi}_1^{\pm} + \bar{q}q'$ as the dominant secondary channel (having the second-largest branching fraction), while 30% have decays to an on-shell second-generation squark + quark as the secondary channel.

The first- and second-generation squark decays are equally insensitive to variations in α. For all α, approximately 50% of models indicate $\tilde{q}_L \to \tilde{g} + q$ is the primary decay channel, while the other 50% have $\tilde{\chi}_1^{\pm} + q'$ as the primary channel. This is also the dominant secondary channel in 48% of the models. Another 40% have $\tilde{\chi}_2^0 + q$ as the secondary channel. The $\tilde{q}_R$ are slightly different, with approximately 62% of models indicating $\tilde{q}_R \to \tilde{g} + q$ as the primary channel, and another 37% $\tilde{q}_R \to \tilde{\chi}_1^0 + q$. This is also the dominant secondary channel in 63% of models, with $\tilde{\chi}_2^0 + q$ the secondary channel for another 32%, and the remaining 5% having $\tilde{q}_R \to \tilde{g} + q$.

Due to dependence on the gaugino mass parameters, the chargino decays are significantly more sensitive to variations of α. For the $\alpha = 0$ case, approximately 74% of models have $\tilde{\chi}_1^{\pm} \to W^{\pm} + \tilde{\chi}_1^0$ as the primary decay channel. Another 25% have $\tilde{\chi}^{\pm} \to \tilde{\chi}_1^0 + \bar{q} + q'$ as the primary channel (here the quarks are from the first or second generation), while the remaining 1% have instead $\tilde{\chi}^{\pm} \to \tilde{\chi}_1^0 + \tau + \nu_{\tau}$. As α increases these three decay channels persist, however their distribution across each set of models begins to change, and additional channels begin to appear. For the $\alpha = 0.33$ case, the above channels occur in 65%, 31%, and 1% of models, respectively. However, now the remaining 3% of models have $\tilde{\chi}_1^{\pm} \to \tilde{\tau}_1^{\pm} + \nu_{\tau}$ as the primary channel. The $\tilde{\chi}^{\pm} \to \tilde{\chi}_1^0 + \bar{q} + q'$ channel is the dominant secondary channel for all α variations.

The $\tilde{\chi}_2^0$ decay behavior is similarly diverse. For case $\alpha = 0$, approximately 39% of models have $\tilde{\chi}_2^0 \to \tilde{\chi}_1^0 + q\bar{q}$ as the primary decay channel, while 23% have $\tilde{\chi}_2^0 \to \tilde{\chi}_1^0 + Z^0$, 28% have $\tilde{\chi}_2^0 \to \tilde{\chi}_1^0 + h^0$, and another 10% have $\tilde{\chi}_2^0 \to \tilde{\chi}_1^0 + \tau^+\tau^-$ as the primary channel. This distribution shifts slightly for $\alpha = 0.33$ to 40%, 26%, 18%, and 13%, respectively. Here, another 3% of models have $\tilde{\chi}_2^0 \to \tilde{\tau}_1^{\pm} + \tau$ as the dominant channel. For $\alpha = 0.66$ it is shifted further to 46%, 18%, 15%, 15%, where here the remaining 3.4% of models now having $\tilde{\chi}_2^0 \to \tilde{\nu}_{eL} + \nu_e$ as the primary channel. For $\alpha = 1.0$, the Z^0 and h^0 decays occur less frequently, with only 8% and 5% of models having these as the primary channel. The $\tilde{\chi}_1^0 + q\bar{q}$, $\tilde{\chi}_1^0 + \tau^+\tau^-$, and $\tilde{\tau}_1^{\pm} + \tau$ channels appear with the largest branching fraction in 56%, 19%, and 9% of models, respectively.

As with the benchmark models, we analyze the 1449 model pairs using the three signature sets given in tables 3, 4 and 5. Due to the large number of model points we present results statistically in the form of the observed distribution of $L_{\min}$. Table 9

JHEP04(2009)114

	$\alpha = 0.33$			$\alpha = 0.66$			$\alpha = 1.0$		
$L_{\min}$ value	List A	List B	List C	List A	List B	List C	List A	List B	List C
≤ 1 fb^{-1}	115	206	282	271	417	474	410	475	484
≤ 2 fb^{-1}	35	93	86	52	36	10	38	9	0
≤ 4 fb^{-1}	49	57	42	52	35	2	24	0	0
≤ 10 fb^{-1}	42	73	50	48	8	0	10	0	0
≤ 100 fb^{-1}	130	40	8	72	0	0	2	0	0
> 100 fb^{-1}	98	0	0	1	0	0	0	0	0

Table 9. **Minimum integrated luminosity $L_{\min}$ to separate $\alpha = 0$ from $\alpha \neq 0$ in controlled model sample.** Distribution of $L_{\min}$ values for the three signature sets of tables 3, 4 and 5. In each case we are comparing the indicated value of α with the case $\alpha = 0$ for the same set of background model parameters.

shows the minimum luminosity required to distinguish between models with $\alpha = 0$ and those with $\alpha \neq 0$ when using, respectively, signature Lists A, B and C. Considering the case of $\alpha = 0.33$ first, signature List A is able to successfully resolve a large number of model pairs with fairly low luminosity. However, only 241 out of the 469 model variations analyzed for this value of α can be resolved with less than 10 fb^{-1}. Signature Lists B and C exhibit significantly stronger resolving power, with List B able to distinguish 429 variations, and List C 461 out of the 469 total model variations considered. Both Lists B and C allow the majority of model variations to be distinguished with ≤ 4 fb^{-1} integrated luminosity, however List C exhibits the best performance overall, as it is able to distinguish the models with a consistently lower luminosity requirement. For the $\alpha = 0.66$ models, all three signature sets allow the majority of model points to be distinguished from $\alpha = 0$ with less than 4 fb^{-1} integrated luminosity. Only List A was unable to resolve all model variations with less than 10 fb^{-1}, as 73 out of 496 models required higher luminosity. Signature List C exhibits the best performance, allowing nearly all model variations to be resolved with ≤ 2 fb^{-1}. The $\alpha = 1.0$ models are sufficiently different from the $\alpha = 0$ case that all three of the signature sets are able to distinguish the two cases with exceptionally low luminosity. Signature List C again exhibits the best performance, allowing all models to be distinguished with less than 1 fb^{-1} of data.

We can understand these results by examining the individual $(R_{AB})_i$ response of each signature. From equation (3.12), the minimum luminosity required to distinguish two models, A and B, is inversely proportional to R_{AB}, which is the sum of the individual $(R_{AB})_i$ values of each signature. Because $(R_{AB})_i$ reflects the sensitivity of the i-th signature to changes between models A and B (a larger $(R_{AB})_i$ value being more sensitive), signatures that have high sensitivity to physical changes associated with α provide a greater contribution to the total R_{AB}, and thus reduce the $L_{\min}$ requirement.

The distribution of R_{AB} values for the single signature of List A is shown in figure 9. For the $\alpha = 0.33$ case the distribution is localized to relatively low values of R_{AB}. For the $\alpha = 0.66$ and $\alpha = 1.0$ cases the distribution begins to spread out, with many models having

JHEP04(2009)114

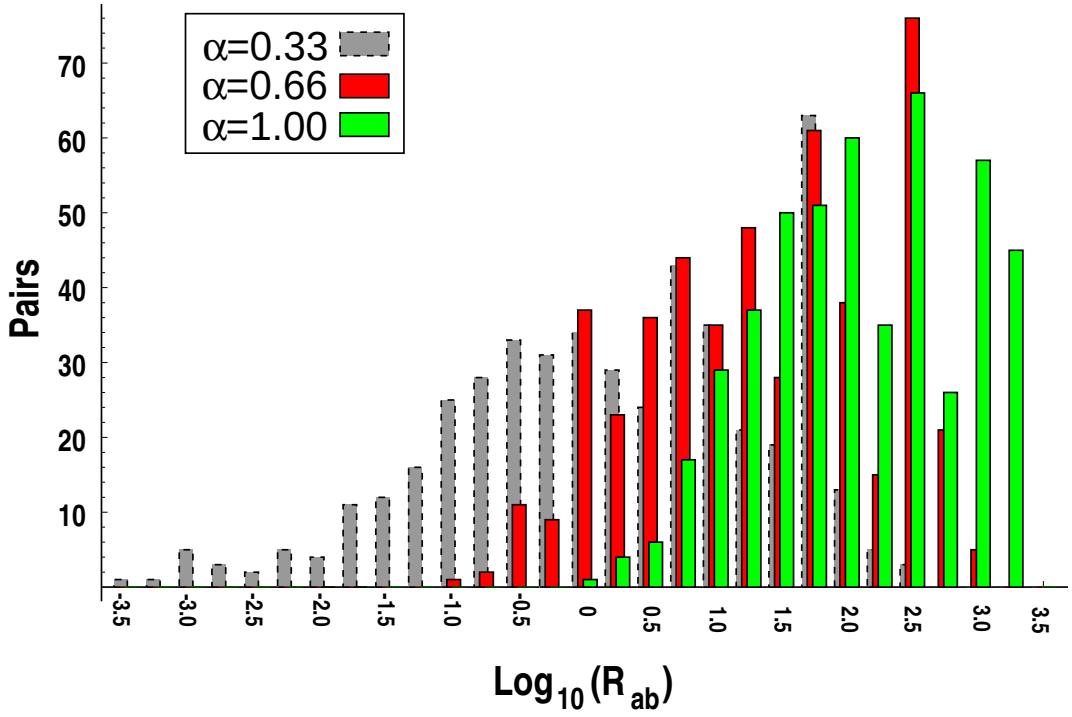

Figure 9. **Distribution of** (R_{AB}) **values for signature List A.** The distribution of R_{AB} values for the single signature of List A is given for the parameter sets $\alpha = 0.33$, $\alpha = 0.66$, and $\alpha = 1.0$. In each case we are comparing the indicated value of α with the case $\alpha = 0$ for the same set of background model parameters. Note that larger values of R_{AB} imply lower values of $L_{\min}$.

significantly larger R_{AB} values. This indicates the signature is becoming increasingly more sensitive to the differences brought on by changes in α as this parameter is increased. However, with only a single signature it is not possible to guarantee that it will be as effective for other models as it is in this example. In order for this approach to work across a broad range of potential physics scenarios it is advantageous to adopt a combination of signatures, where each may be sensitive to one or more aspects of a particular class of models.

Figures 10 and 11 show the distributions of $(R_{AB})_i$ obtained for the five signatures of signature List B. Each figure represents five histograms where the variable being considered is $\log_{10}[(R_{ab})_i]$, with the comparison being between $\alpha = 0$ and $\alpha = 0.33$ in figure 10 and between $\alpha = 0$ and $\alpha = 1$ in figure 11. In a similar fashion to the single signature of List A, the distributions are in general clustered at low $(R_{AB})_i$ for $\alpha = 0.33$, and begin to spread out considerably, taking on much larger values as α increases. Comparing the individual distributions to those in the single signature of List A, the overall spread of values is not significantly different. However, recall that R_{AB} is the sum of the individual $(R_{AB})_i$ values. Therefore we gain a significant enhancement by simply including additional signatures. A similar effect occurs with the larger set of signatures in List C. As we saw in section 3, however, there is ultimately a point of negative returns and a maximum efficacy

JHEP04(2009)114

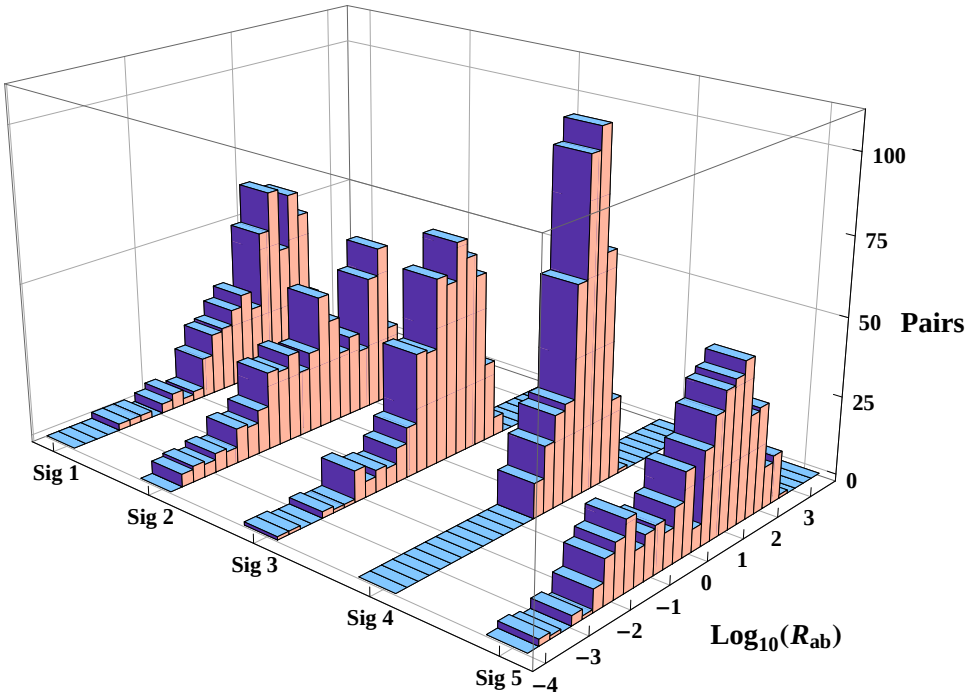

Figure 10. **Distribution of $(R_{AB})_i$ values for signature List B [$\alpha = 0.33$ versus $\alpha = 0$].** The distribution of $(R_{AB})_i$ values for the five signatures of List B is given for the case of comparing $\alpha = 0$ with $\alpha = 0.33$. For the definition of the five signatures, see table 4.

is obtained.

Thus far we have presented the results of our approach in terms of the minimum integrated luminosity required to resolve two model classes ($\alpha = 0$ and $\alpha \neq 0$) using our set of optimized signatures. To understand why this approach works, it is useful to examine the signature results themselves. Figures 12 and 13 show examples of two-dimensional slices of the signature space "footprint" for our large set of model variations. In these figures the results have been normalized to 5 fb^{-1} of data.

Figure 12 compares the count rates for the third and fourth signatures of List B for the case $\alpha = 0$ versus $\alpha = 0.66$ (left panel) and $\alpha = 1$ (right panel). Figure 13 compares the count rates for signatures #11 and #13 of List C for the case $\alpha = 0$ versus $\alpha = 0.66$ (left panel) and $\alpha = 1$ (right panel). In this case the two signatures are both taken from the set of events containing at least one lepton and five or more jets (see table 5). We have chosen this pair for the dramatic separation that can be achieved, though similar results can be obtained with other pairs of signatures.

The power of our inclusive signature list approach lies in the choice of signatures and their ability to remain highly sensitive to changes in the physical behavior of each model. This feature is reflected qualitatively in the visual clustering of the data points, which become progressively more distinct as the parameter α is increased. As the regions separate it becomes increasingly less likely that a model from one class can be confused with a model from the other class, even when considering statistical fluctuations. In our

JHEP04(2009)114

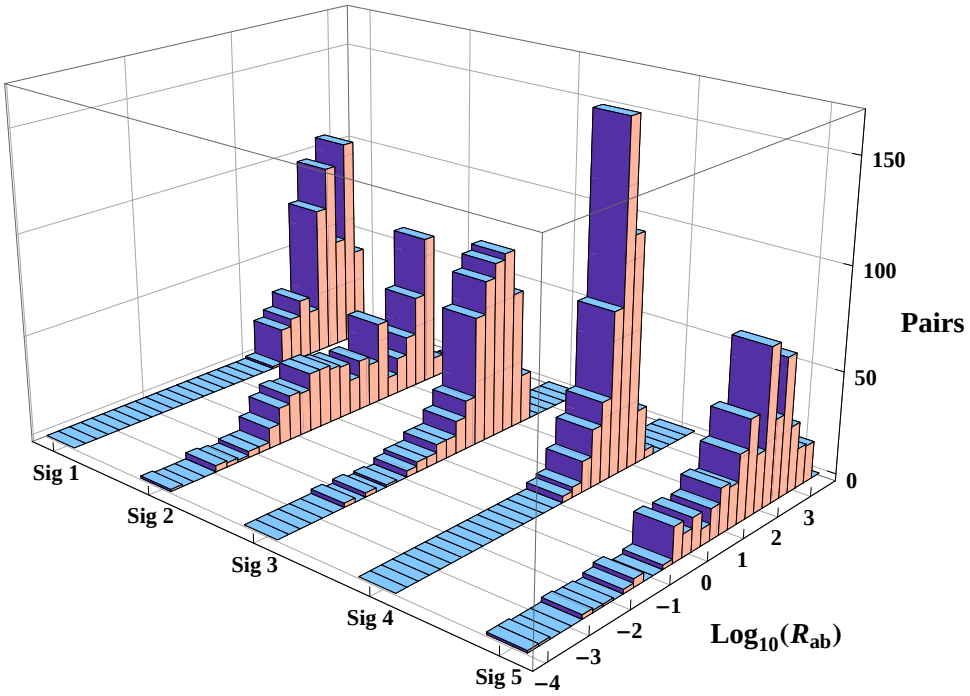

Figure 11. **Distribution of $(R_{AB})_i$ values for signature List B [$\alpha = 1$ versus $\alpha = 0$].** The distribution of $(R_{AB})_i$ values for the five signatures of List B is given for the case of comparing $\alpha = 0$ with $\alpha = 1$. For the definition of the five signatures, see table 4.

approach this manifests itself when one computes R_{AB}, which reflects the "distance" in signature space between the two models under comparison, and which becomes large when the models are sufficiently different from one another.

The idea of using repeated pairings of targeted observables in order to separate model classes was studied in previous "footprint-style" analyses [47–49]. If we consider the universal gaugino mass scenario (i.e. $\alpha = 0$) as a "model," and the case of non-universal gaugino masses as a separate model, then a set of signatures will be truly targeted at this particular model feature if the set of all such two-dimensional planes implies complete separation between the models. With this in mind it is interesting to examine distinguishability between the two values of α from a somewhat different perspective. Adopting the approach of [49] we can ask how many degeneracies exist between the two classes of models, where by degeneracy we mean two models that exist at different points in the microscopic parameter space, but occupy the same point in signature space (up to statistical fluctuations). If it is possible, through application of one or more signatures, to ensure that no degeneracies exist we can claim to that it is possible to completely discriminate between the two classes.

As an example of how this idea can be applied, we can consider the analysis performed in [49]. Let one particular value of the parameter α (such as $\alpha = 0$) be "model A" and let some other value of the parameter α be "model B." Choose any pair of signatures in one of the signature lists. From our controlled sample we can choose an individual case $B_j \in B$ and compute the quantity $(\Delta S_{A_i B_j})^2$ between that particular point and all the

JHEP04(2009)114

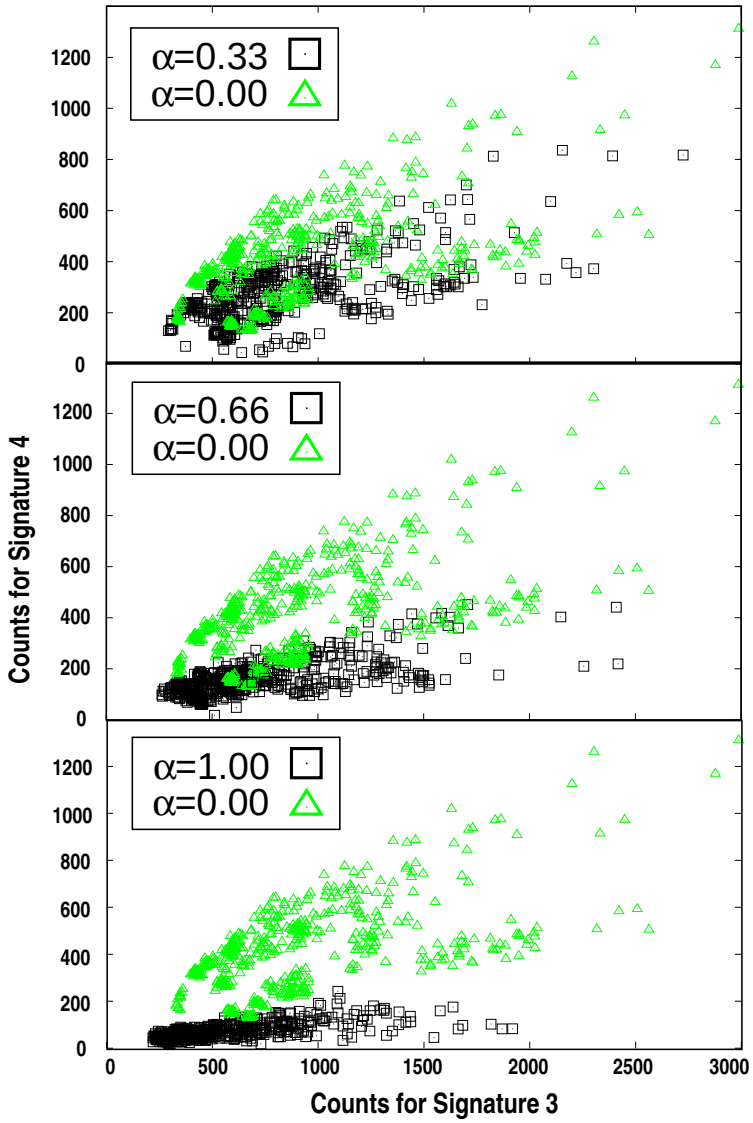

Figure 12. Footprint-style plot for a pair of signatures from List B. Total counts for signature #3 versus signature #4 of List B is given for the case $\alpha = 0$ (green triangles) $\alpha \neq 0$ (black squares). The cases shown are for $\alpha = 0$ versus $\alpha = 0.33$ (top panel), $\alpha = 0.66$ (middle panel) and $\alpha = 1$ (bottom panel). The axes measure the number of events for which the kinematic quantity was in the range given in table 4. Larger values of the non-universality parameter α correspond to a greater degree of separation between the two model "footprints."

points $A_i \in A$ for this pair of signatures. If the value for all such $(\Delta S_{A_i B_j})^2$ is always greater than the two-signature threshold given by $\gamma_2(0.95)$ in table 10 we will claim the point B_j has been separated from the entire footprint of model A. We can then repeat this exercise over all cases of model B. The number of cases of model B that have *not* been separated from the entire footprint of model A we will denote as N_{BA}. This is a type of degeneracy count for model B with respect to model A. Clearly the process can

JHEP04(2009)114

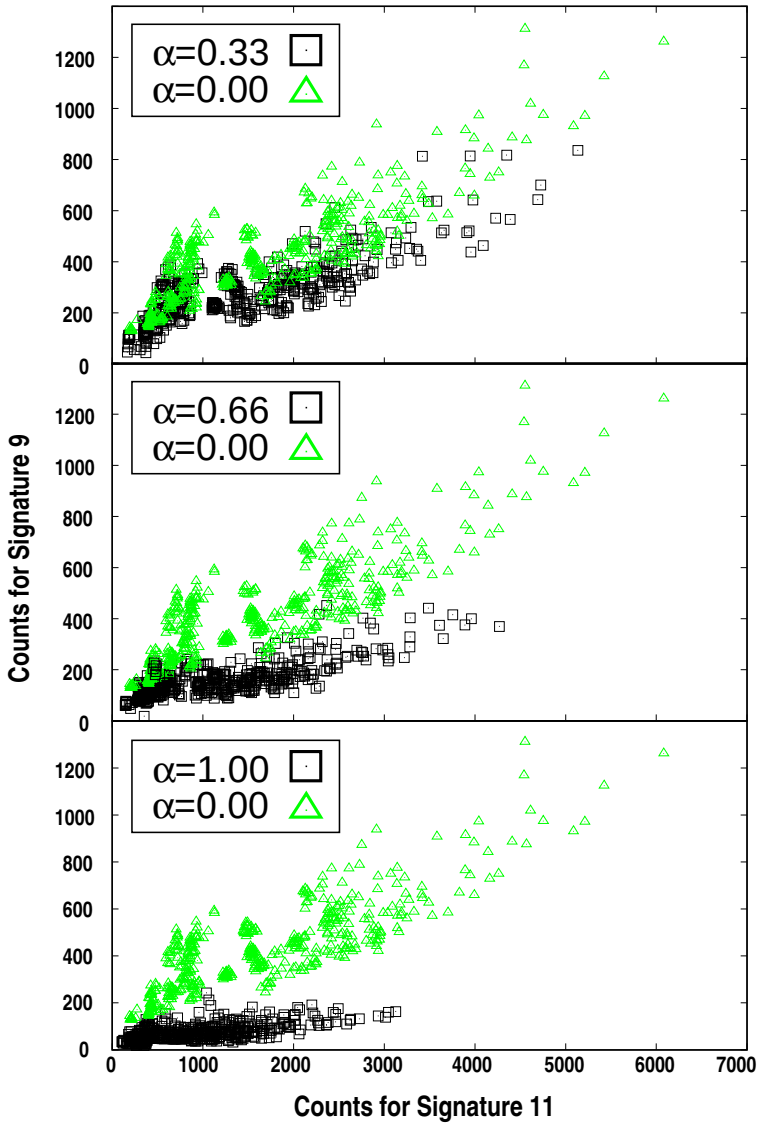

Figure 13. **Footprint-style plot for a pair of signatures from List C.** Total counts for signature #11 versus signature #13 of List C is given for the case $\alpha = 0$ (green triangles) $\alpha \neq 0$ (black squares). The cases shown are for $\alpha = 0$ versus $\alpha = 0.33$ (top panel), $\alpha = 0.66$ (middle panel) and $\alpha = 1$ (bottom panel). The axes measure the number of events for which the kinematic quantity was in the range given in table 5. Larger values of the non-universality parameter α correspond to a greater degree of separation between the two model "footprints."

be performed for model A with respect to model B, producing a degeneracy count N_{AB}. In general we expect these two numbers to be roughly equivalent in magnitude, but not necessarily precisely equal.

If either N_{AB} or N_{BA} are non-vanishing then the two footprints are not yet disjoint in the multi-dimensional signature space. We can then choose any other pair of signatures and repeat the procedure, this time restricting A_i and B_j to run only over the degenerate

JHEP04(2009)114

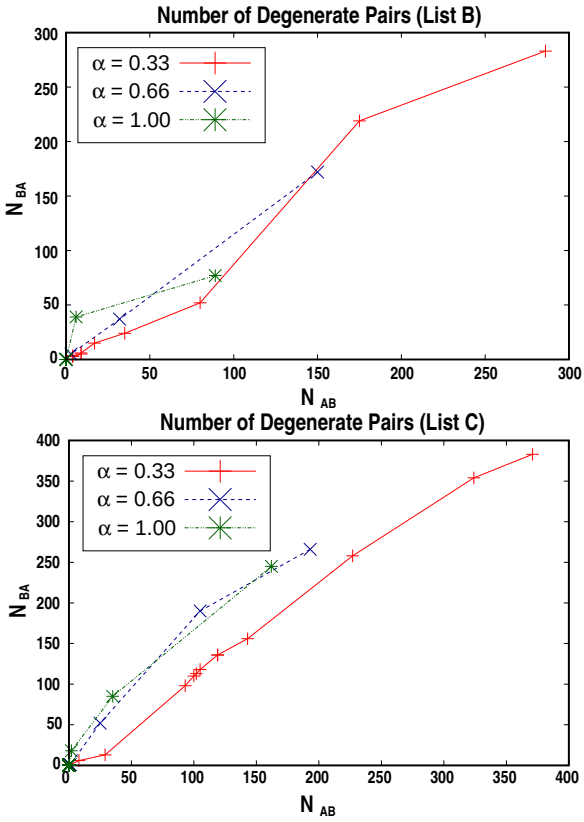

Figure 14. Degeneracy counts for List B (left panel) and List C (right panel). The relative degeneracy counts N_{AB} and N_{BA} that result from successive application of pairs of signatures from List B and List C are plotted for our controlled model sample. In each case model A is the case with $\alpha = 0$ while model B is the case with the indicated value of $\alpha \neq 0$. Once all model pairs have been applied the total degeneracy count vanishes for both lists and for all values of $\alpha \neq 0$.

cases. If we have chosen a good set of signatures the quantities N_{AB} and N_{BA} should rapidly converge to zero as the algorithm is successively applied. The results of performing this exercise on the controlled model sample generated by the parameters of table 7 is shown in figure 14. In the left panel we show the successive values of N_{AB} and N_{BA} as pairs of signatures from List B are used to compute the separability parameter $(\Delta S_{AB})^2$, while the right panel uses pairs of signatures from List C. In both cases "model A" represents the set of models with $\alpha = 0$, while "model B" represents the case with the indicated value of $\alpha = 0.33$, 0.66 and 1.0. For all three values of the parameter α the lists do an excellent job of converging towards $N_{AB} = N_{BA} = 0$ after only a few pairings are considered. This suggests that the signature lists of tables 4 and 5 should be able to reveal the departure of the gaugino soft masses from the universal ratios on a truly *general* supersymmetric model with a high degree of reliability and in a small amount of integrated luminosity.

To honestly confirm this hypothesis we must generate a more random set of models. After all, the signature lists of tables 3, 4 and 5 were constructed precisely with the sorts of models of our controlled sample in mind. But as we saw in section 4.1, models such as

JHEP04(2009)114

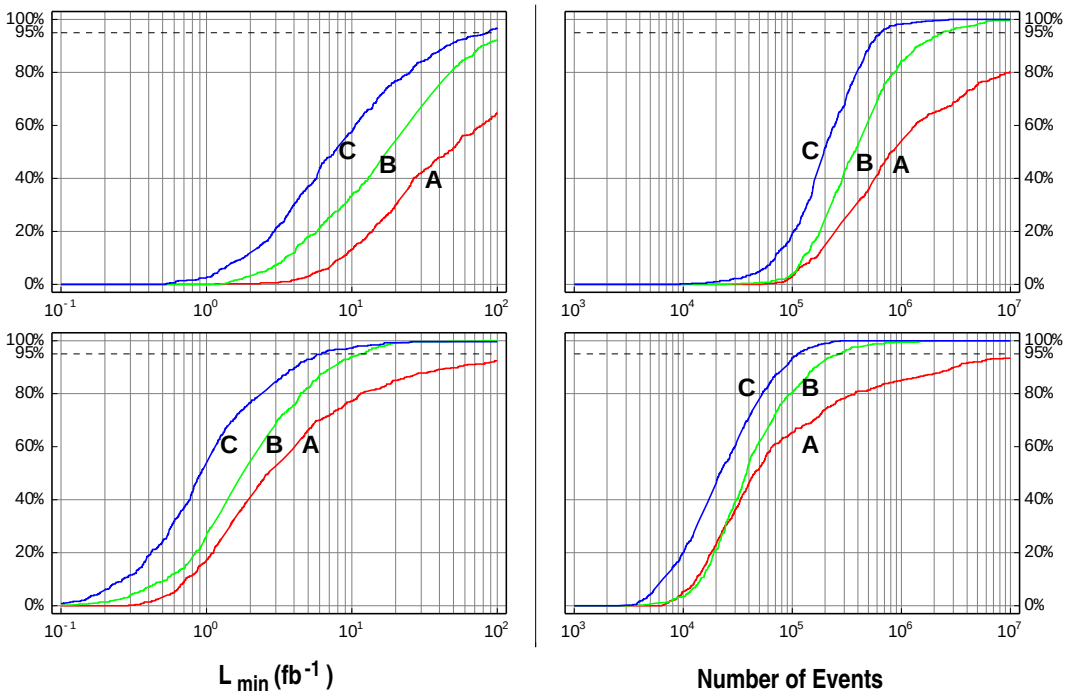

Figure 15. **Efficiencies of the three signature lists.** The ability of the three signature lists to separate the case $\alpha = 0.1$ from $\alpha = 0$ is indicated in the top pair of plots and the simpler case $\alpha = 0.3$ from $\alpha = 0$ in the bottom pair of plots. On the left, the percentage of cases that could be distinguished using each of the three signature lists of tables 3, 4 and 5 is given as a function of integrated luminosity in units of fb^{-1}. On the right the same percentage is shown as a function of the number of supersymmetric events. The 95% separability threshold is indicated by the dashed horizontal line.

benchmark model A can prove more challenging for our analysis algorithm. To allow for the possibility of more perverse cases than those of our controlled sample, an additional set of 500 models were generated with six points on the α-lines ranging from 0 to 0.5. In this case a 16-dimensional parameter space defined by the quantities in (3.1) was considered. Specifically, slepton and squark masses were allowed to vary in the range 300 GeV to 1200 GeV with the masses of the first and second generation scalars kept equal. The gaugino mass scale given by M_3 and the μ-parameter were also allowed to vary in this range. The pseudoscalar Higgs mass m_A was fixed to be 850 GeV and the value of $\tan\beta$ was allowed to vary from 2 to 50. If all points along the α-line satisfied all experimental constraints on the superpartner mass spectrum, then 100,000 events were generated for each of the six points along the α-line in the manner described in section 3. Using this data the value of $L_{\rm min}$ was computing using (3.13) and (3.14) for each of our three signature sets.

The results of this analysis are given in figures 15 and 16. Figure 15 considers the ability of our signature lists to separate the case $\alpha = 0.1$ from $\alpha = 0$ (top pair of plots) and the simpler case $\alpha = 0.3$ from $\alpha = 0$ (bottom pair of plots). On the left, the percentage of cases that could be distinguished using each of the three signature lists of tables 3, 4 and 5

JHEP04(2009)114

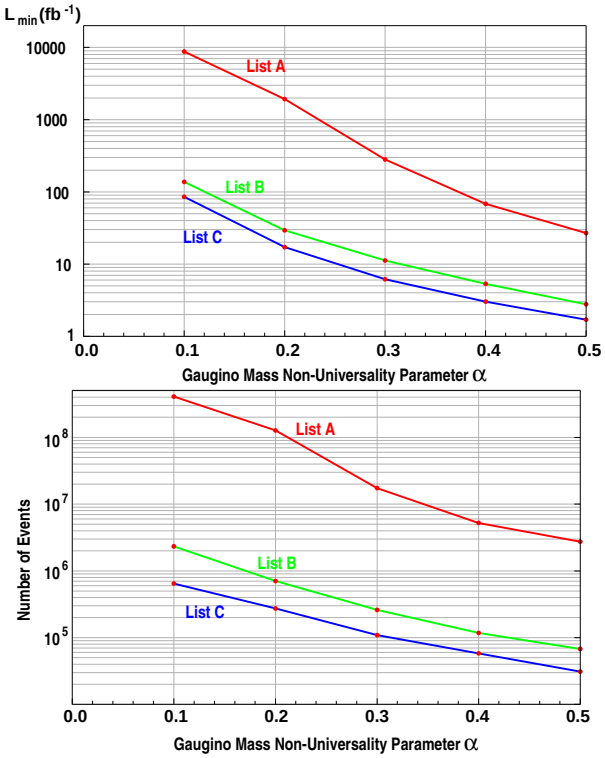

Figure 16. $L_{\min}$ **and** $N_{\min}$ **required to detect** $\alpha \neq 0$ **for 95% of the random models.**

is given as a function of integrated luminosity in units of fb^{-1}. Since the random model sample includes examples with very different superpartner mass scales, the overall supersymmetric production cross-section varies much more across this sample than in the controlled model sample described above. We therefore take this into account by plotting the same percentage in terms of the number of supersymmetric events on the right side of figure 15. The 95% separability threshold is indicated by the dashed horizontal line. Even using our best set of signatures (List C) it will require nearly 100 fb^{-1} to be able to detect non-universality at the level of $\alpha \simeq 0.1$ for an arbitrary supersymmetric model. Yet for the vast majority of models the departure from universality should become apparent after just 10-20 fb^{-1}. Departures from universality at the level of $\alpha \simeq 0.3$ should be apparent using this method for most supersymmetric models after just a few fb^{-1}. In figure 16 the integrated luminosity (or number of supersymmetric events) needed to detect $\alpha \neq 0$ for 95% of our random models is given as a function of the five non-vanishing α values simulated.

5 Conclusions

If supersymmetry is discovered at the LHC the high energy community will be blessed with a large number of new superpartners whose masses and interactions will need to be measured. At the same time the community will be cursed by a large model space with many Lagrangian parameters which cannot themselves be directly measured experimen-

JHEP04(2009)114

tally. Undoubtedly performing global fits of the many observables to the parameter space of certain privileged and well-defined benchmark models will be of great help in making sense of this embarrassment of richness. But recent work suggests that unless these models are determined by very few parameters it is likely (if not perhaps inevitable) that multiple points in the parameter space will fit the data well. It then becomes an interesting question to ask whether it is possible to fit to certain model *characteristics* rather than to any particular model itself.

In our opinion one of the most important such characteristic is the pattern of soft supersymmetry-breaking gaugino masses. No other property of the low-energy soft Lagrangian is more easily linked to underlying high-scale physics, particularly if that high-scale physics is of a string-theoretic origin. Only the related issue of the wavefunction of the LSP is of more importance to low-energy physics and cosmology. We are thus interested in asking whether we can identify the presence on non-universalities in the gaugino sector independent of all other properties of the superpartner spectrum. The manner by which any such undertaking can be tackled is by no means clear — though neither is it clear that such an undertaking is inherently impossible. In the present work we have decided to begin this process with a simple parametrization of the gaugino masses determined by a single parameter which can be thought of as the ratio of bulk gravity and anomaly contributions to gaugino masses. We developed model "lines" in the spirit of previous benchmark studies such as the Snowmass Points & Slopes in which only the single non-universality parameter is varied. By understanding how the observable physics at the LHC is affected by this parameter — and then repeating the analysis many times with the other supersymmetric parameters varied — we can learn which LHC signatures are most directly "targeted" at this important underlying characteristic.

Our procedure depends on certain analytic results that in turn depend on the assumption that the signatures considered have fluctuations which are largely uncorrelated with one another. This severely limits the type of signature ensembles one might construct. Yet this restriction does not imply a loss of resolving power, as the "optimal" signature list is rarely the largest possible list one can imagine. Our analysis has suggested two signatures ensembles which perform remarkable well at the task of measuring the value of the non-universality parameter we introduce. The larger of the two generally performed slightly better, but at the expense of allowing signatures that are correlated with one another at the 30% level. Requiring a correlation at only the 10% level (and thus using a shorter list of observables) had only a small effect on the ability to distinguish the size of the non-universality parameter α. Broadly speaking, we find that a non-universality at the 10% level can be measured with 10-20 fb^{-1} of integrated luminosity over approximately 80% of the supersymmetric parameter space relevant for LHC observables. If we are interested in measurements at only the 30% level these numbers change to 5-10 fb^{-1} over approximately 95% of the relevant parameter space.

This is remarkable progress, but the task we set out for ourselves is admittedly still somewhat artificial. There are two independent mass ratios that can be constructed from the three soft supersymmetry breaking gaugino masses — our parametrization is therefore not fully general. It would be of great interest to study more general departures from non-

JHEP04(2009)114

universality to see if the optimal signature lists change substantially. Of greater import is the need to perform a Monte Carlo simulation in order to compare a candidate model to the "data" at the LHC. To perform such a comparison we must assume knowledge of all input parameters *apart* from the one we are attempting to measure. While this is a common practice in benchmark studies at colliders, it is far from the reality that theorists and experimentalists will encounter in the early stages of the LHC era. Our study demonstrated the efficacy of certain targeted observables in extracting the non-universality parameter α while keeping all other parameters fixed for the two models. This is quite a strong assumption and future work should relax this constraint. In other words, one would like to distinguish between two models (with different values of α) even if the other parameters for the two models are not the same. There are many directions by which this may be pursued. For example, in the current analysis we have not allowed ourselves any knowledge of the mass spectrum, though analysis of kinematic end-points will certainly provide some information in this regard early on in LHC data-taking. In addition, techniques such as the use of on-shell effective theories [50] might provide sufficient information about the dominant production and decay modes for new mass eigenstates to allow an approximation to our analysis to be performed before the full mass spectrum is reconstructed. We hope to pursue both avenues for introducing greater realism in future work.

Acknowledgments

The authors would like to thank Piyush Kumar for important discussions at the beginning of this project. B.A. and B.D.N. would like to thank the Michigan Center for Theoretical Physics for hospitality during the early stages of this work. B.A., M.H. and B.D.N. are supported by National Science Foundation Grant PHY-0653587.

A Some specific examples

The low energy limit of four-dimensional string constructions can be studied as a supergravity theory defined by three functions of the massless chiral superfields: the Kähler potential K, the superpotential W and the gauge kinetic function f_a. As in the previous subsection the label a refers to a particular gauge group $\mathcal{G}_a$. This last function is naturally of most import for the soft supersymmetry breaking gaugino masses, but all three functions play a role in determining the nature of supersymmetry breaking in the observable sector. In string models the gauge kinetic function is typically determined by gauge-singlet chiral superfields which we will simply refer to as moduli. The Kähler potential and superpotential are generally functions of both moduli and gauge-charged matter superfields.

Let us assume, as is so often the case at tree-level in string theory models, that the gauge kinetic function is linear in the moduli[7]

$$f_a = k_a X_a \,. \tag{A.1}$$

[7]Unless explicitly written otherwise, in this appendix we are always using Planck units in which $M_{\rm PL} = 1$.

JHEP04(2009)114

Here X_a represents a generic modulus field and we have allowed for the possibility that each gauge group can have its own modulus dependence. The proportionality constant k_a can be thought of as the affine level at which the gauge group $\mathcal{G}_a$ is realized in the underlying conformal field theory. We will hereafter always set this constant to unity. Note that the real part of the lowest (scalar) component of X_a must acquire a vacuum expectation value (VEV) in order to determine the size of the corresponding gauge coupling

$$< \mathrm{Re}\ x_a > = \frac{< x_a + \bar{x}_a >}{2} = \frac{1}{g_a^2}, \tag{A.2}$$

where $x_a = X_a|_{\theta=\bar{\theta}=0}$. If we wish to entertain the notion of gauge coupling unification then we must either arrange these VEVs to be equal, or there must be a single universal modulus X to couple to all gauge groups with equal strength. The latter is the case for the two models we will consider below so we will assume

$$f_a = X; \qquad < \mathrm{Re}\ x > = 1/g_{\mathrm{STR}}^2, \tag{A.3}$$

where g_{STR} is the universal gauge coupling at the string scale. The highest component of the chiral superfield X is the auxiliary field F^X. A non-zero expectation value for this field, or indeed of any other such auxiliary field, is an indication of spontaneous breaking of supersymmetry. The manifestation of this supersymmetry breaking in the form of gaugino masses is given (at tree level) by the expression

$$M_a = \frac{g_a^2}{2} F^N \partial_N f_a, \tag{A.4}$$

where the repeated index n sums over all chiral superfields present in the function f_a and the expression on the left is understood to be evaluated in the vacuum. For the case of (A.3) this implies

$$\begin{aligned} M_a &= \frac{g_{\mathrm{STR}}^2}{2} F^X \\ &= \left\langle \frac{F^X}{x + \bar{x}} \right\rangle , \end{aligned} \tag{A.5}$$

where in the last line we have made explicit the vacuum evaluation at the string scale. Now we have arrived at a universal contribution to the three gaugino masses of the Standard Model, which gives rise to the term $M_a^1(\Lambda_{\mathrm{UV}})$ of (2.1).

Additional contributions to (A.4) appear at the loop level. The structure of these terms have been computed elsewhere [35, 36, 51] and they generally depend on details of the complete theory beyond the form of the tree level gauge kinetic function. A subset of these terms can be derived completely from the superconformal anomaly, the most important of which is universal for any supergravity theory

$$M_a|_{\mathrm{an}} = -\frac{g_a^2(\Lambda_{\mathrm{UV}})}{2} \frac{b_a}{16\pi^2} \frac{2\overline{M}}{3} . \tag{A.6}$$

The coefficient b_a is as defined in (2.3) and the field M is the auxiliary field of the supergravity multiplet whose expectation value determines the gravitino mass $m_{3/2} = -\frac{1}{3} \langle \overline{M} \rangle$.

In the limit where this is the *only* significant one loop correction to the gaugino masses we recover the expression in (2.2) where $M_g \equiv m_{3/2}$.

We now have our two components to the mirage gaugino mass pattern. Our next task is to ask how the magnitudes of $M_u = \langle F^X/(x+\bar{x})\rangle$ and $M_g = -\langle \overline{M}\rangle/3$ might be related to one another. As both F^X and M are auxiliary fields their equations of motion are easy to obtain, relating these quantities to the Kähler potential and superpotential via

$$F^M = -e^{K/2}K^{M\overline{N}}\left(\overline{W}_{\overline{N}} + K_{\overline{N}}\overline{W}\right), \quad \overline{M} = -3e^{K/2}\overline{W} \tag{A.7}$$

with $W_{\overline{N}} = \partial W/\partial\overline{Z}^{\bar{N}}$, $K_{\overline{N}} = \partial K/\partial\overline{Z}^{\bar{N}}$ and $K^{M\bar{N}}$ being the inverse of the Kähler metric $K_{M\overline{N}} = \partial^2 K/\partial Z^M \partial\overline{Z}^{\bar{N}}$. Here Z^N represents any chiral superfield, including our particular modulus X from the gauge kinetic functions. Given a specific model of supersymmetry breaking — such as gaugino condensation — the modulus dependence on the non-perturbatively generated superpotential terms can be computed and (A.7) can be used to explicitly relate the size of the gravitino mass to the size of $\langle F^X\rangle$. However, if we make the assumption that the scalar potential has vanishing vacuum expectation value in the ground state of the theory then we can bypass this complication and use this assumed constraint directly [52]. The scalar potential is given by

$$V = K_{M\overline{N}}F^M\overline{F}^{\bar{N}} - \frac{1}{3}M\overline{M} \tag{A.8}$$

where repeated indices are again summed. The condition $\langle V\rangle = 0$ immediately relates the auxiliary F-terms to the gravitino mass. In particular, if F^X is the only non-vanishing F-term component in the theory then we have

$$\langle F^X\rangle = \sqrt{3}m_{3/2}\left\langle (K_{x\bar{x}})^{-1/2}\right\rangle, \tag{A.9}$$

up to a possible phase. For the moduli we will consider in this paper the tree level Kähler potential is typically $K_{\rm tree}(X,\overline{X}) = -\ln(X+\overline{X})$ and thus the imposition of vanishing scalar potential in the vacuum implies

$$M_u = \left\langle \frac{F^X}{(x+\bar{x})}\right\rangle = \sqrt{3}m_{3/2} = \sqrt{3}M_g\,. \tag{A.10}$$

Clearly such a situation will *not* result in the ratio $r = M_g/M_u \sim \mathcal{O}(10-100)$ and therefore if (A.10) holds the contribution from (A.6) will be only a small perturbation on the universal contribution from (A.5).

But this is where a thorny "problem" for string phenomenology becomes an opportunity. The problem is that the vast majority of simple, explicit models of dynamical supersymmetry breaking (such as the gaugino condensation mentioned above) do not produce vanishing vacuum energy. In other words, when the values of $m_{3/2}$ and $\langle F^X\rangle$ are computed from first principles via (A.7) the relation in (A.9) typically fails to be true. This is often considered an embarrassment for string models and much effort in string phenomenology is devoted to stabilizing moduli and breaking supersymmetry while simultaneously achieving $\langle V\rangle = 0$. While many solutions have been postulated through the years, we can group them

JHEP04(2009)114

here into two broad classes. In the first class the simple structure of the scalar potential in (A.8) is retained, with a single modulus carrying non-vanishing auxiliary VEV, but the Kähler potential is assumed to differ from the tree level form $K_{\rm tree}(X,\overline{X}) = -\ln(X+\overline{X})$ so that (A.10) is modified and $\langle V\rangle = 0$ is obtained. For the second class a new sector is brought into the theory to produce a new contribution to the scalar potential δV of approximate magnitude $\delta V \simeq m_{3/2}^2$. If this new sector does not interact with the observable sector then its sole impact is to approximately cancel the large (negative) vacuum energy associated with the second term in (A.8), leaving $\langle F^X\rangle$ essentially disconnected from the size of the gravitino mass. As we will see below, explicit examples of both classes of solutions have the remarkable property of giving rise to the same general pattern of gaugino masses as in (2.14).

A.1 Class 1: Kähler stabilization models

As an example of the first class of models we will consider the weakly coupled heterotic string models studied by Binetruy, Gaillard and Wu (BGW) [53, 54] and reviewed in [29]. The presentation here will follow that of [37] from which we will take our benchmark scenario.

For the heterotic string gauge coupling unification is a result of a single modulus, the dilaton S, appearing universally in all gauge kinetic functions. The BGW construction postulates the existence of some non-perturbative correction to the action for the dilaton field, along the lines of that originally suggested by Shenker [55], which results in a modification of the Kähler metric for the dilaton scalar. Borrowing the notation of (A.9) with $X \to S$ it is sufficient for our purposes to parameterize this modification as follows

$$F^S = \sqrt{3}m_{3/2}(K_{s\bar{s}})^{-1/2} = \sqrt{3}m_{3/2}a_{\rm np}(K^{\rm tree}_{s\bar{s}})^{-1/2}, \tag{A.11}$$

where we have introduced the parameter

$$a_{\rm np} \equiv \left(\frac{K^{\rm tree}_{s\bar{s}}}{K^{\rm true}_{s\bar{s}}}\right)^{1/2} \tag{A.12}$$

designed to measure the departure of the dilaton Kähler potential from its tree level value. Recall that $\langle (K^{\rm tree}_{s\bar{s}})^{1/2}\rangle = \langle 1/(s+\bar{s})\rangle = g^2_{\rm STR}/2 \simeq 1/4$ and $s = S|_{\theta=\bar{\theta}=0}$.

In order to be more concrete we must build a model for supersymmetry breaking in which $a_{\rm np}$ is calculable. Here we will take an indirect approach. Consider the field-theoretic non-perturbative phenomenon of gaugino condensation. Using the relation between the dilaton and the gauge coupling it is easy to see that the effective superpotential generated by the gaugino condensate will have the form $W(S) \propto (e^{-(8\pi^2/b_a)S})^3$ were b_a is the beta-function coefficient of a condensing gauge group $\mathcal{G}_a$ of the hidden sector. Let us simplify things by assuming a single condensing gauge group, which we will denote by $\mathcal{G}_+$, with beta-function coefficient $b_+ = b_a/16\pi^2$. The values of b_+ can be quite a bit larger than analogous values for the Standard Model groups, but a limiting case for the weakly coupled heterotic string is that of a single E_8 gauge group condensing in the hidden sector, so that $\mathcal{G}_+ = \mathcal{G}_{E_8}$ and $b_+ = 90/16\pi^2 = 0.57$. Clearly we must insist $b_+ > 0$ in order for gaugino condensation to happen at all.

JHEP04(2009)114

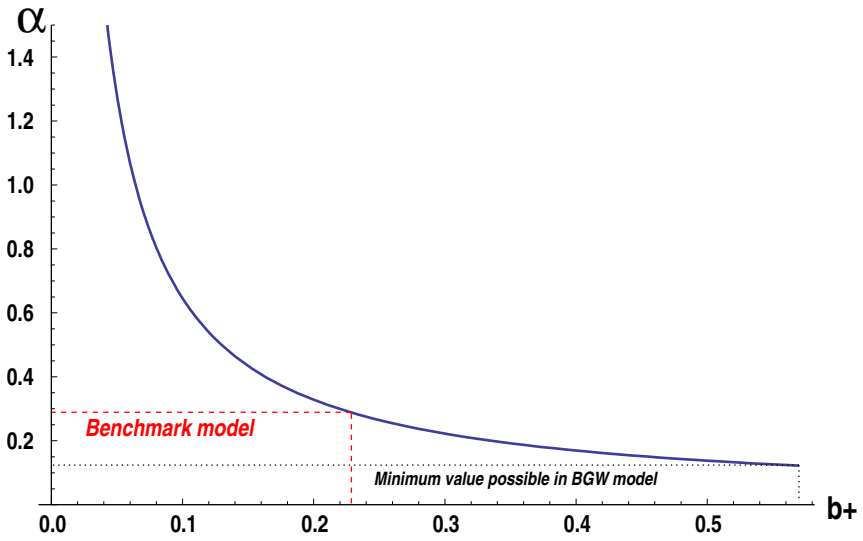

Figure 17. **Effective value of α as a function of b_+ in the BGW class of models.** The parameter b_+ represents the beta-function coefficient of the largest gauge group which experiences gaugino condensation in the hidden sector. This parameter controls the effective value of α for the gaugino masses at the electroweak scale. Since the largest possible confining group would be E_8 there is a minimal size to the effective α parameter in this class of theories. The benchmark point considered in the text corresponds to $b_+ = 36/16\pi^2$.

However, if we do not insist on the tree level dilaton Kähler potential then the vanishing of the vacuum energy implies [56]

$$(K_{s\bar{s}})^{-1}\left|K_s - \frac{3}{2b_+}\right|^2 = 3 \quad \rightarrow (K_{s\bar{s}})^{-1/2} = \sqrt{3}\frac{\frac{2}{3}b_+}{1-\frac{2}{3}b_+K_s}\,, \tag{A.13}$$

where we have used the equations of motion (A.7) for F^S and $W(S) = e^{-3S/2b_+}$. So provided $K_s \sim \mathcal{O}(1)$ so that $K_s b_+ \ll 1$ we can immediately see that a Kähler potential which stabilizes the dilaton while simultaneously providing zero vacuum energy will necessarily imply a suppressed dilaton contribution to soft supersymmetry breaking. Indeed, from (A.12)

$$a_{\rm np} = \sqrt{3}\frac{\frac{2}{3}\frac{g^2_{\rm STR}}{2}b_+}{1-\frac{2}{3}K_s b_+} \ll 1, \tag{A.14}$$

and

$$r = M_g/M_u = m_{3/2}\left\langle\frac{(s+\bar{s})}{F^S}\right\rangle = \frac{1}{\sqrt{3}a_{\rm np}} \gg 1\,. \tag{A.15}$$

It is not hard to construct explicit examples which achieve the outcome in (A.13) and (A.14) [57, 58].

The value of the parameter α associated with (A.15) can be readily computed from (2.13)

$$\alpha = \frac{1}{\sqrt{3}\ln\left(M_{\rm PL}/m_{3/2}\right)a_{\rm np}}\,. \tag{A.16}$$

Using (A.14) and the assumption that $\langle K_s \rangle = -g_{\rm STR}^2/2$ we can plot the predicted value of α as a function of condensing group beta-function coefficient b_+. The result is shown in figure 17. Note that the largest possible value of b_+ ($b_+ = b_{E_8} = 90/16\pi^2 = 0.57$) corresponds to the smallest possible α value. We immediately see that if this class of models is realized in Nature then the $\alpha \to 0$ limit cannot be obtained and *departures from the mSUGRA gaugino mass regime are a prediction of the theory.* Our benchmark point will take $b_+ = 36/16\pi^2$ which corresponds to $a_{\rm np} = 1/15.77$. Such a value for b_+ could arise from a condensation of a sector consisting only of E_6 Yang-Mills fields and no matter charged under the E_6 group. This benchmark point was studied in [37] and we give the explicit soft supersymmetry breaking mass parameters for the point in table 1 at the end of this appendix.

The corresponding effective α value at the scale $\Lambda_{\rm EW} = 1$ TeV is $\alpha = 0.28$. We note that extraction of the value of α from low-scale gaugino soft masses depends on the renormalization group scale, as is apparent from expressions such as (2.11) and (2.14). In particular, the value of $\alpha = 0.28$ can be extracted using the ratios in (1.1) provided the gaugino masses are evaluated at the scale $\Lambda_{\rm EW} = 1$ TeV. The value of α at other scales can be found by using the more general formula (2.11).

A.2 Class 2: Type IIB models with flux compactifications

The second type of solution to the vacuum energy problem — introducing a new sector whose purpose is to cancel negative contributions to the vacuum energy arising from the last term of (A.8) — is realized in certain constructions of Type IIB string theory compactified on Calabi-Yau orientifolds [27]. In this class of theories NS and RR three-form fluxes are introduced to stabilize many of the moduli upon compactification. The presence of this flux warps the bulk geometry of the Calabi-Yau, resulting in a "throat" of the Klebanov-Strassler type [59]. At the infrared end of this throat a hidden sector gaugino condensate exists on a set of D_7-branes and is thus "sequestered" from the observable sector, in the language of Randall and Sundrum [26]. For gauge theories living on D_7 branes the gauge coupling is determined by the Kähler modulus T, as opposed to the dilaton S of the heterotic example presented previously. But apart from this small notational change much of the phenomenology is strikingly similar to the example in the previous subsection.

The Kähler potential for the modulus T is again taken to be $K = K_{\rm tree}(T, \overline{T}) = -\ln(T + \overline{T})$ and we assume that the Standard Model exists on a second collection of D_7 branes such that the (tree level) gauge kinetic functions for the Standard Model gauge groups are universal and of the form $f_a = T$. In the effective supergravity theory just below the string compactification scale, the presence of the three-form fluxes is represented by a constant W_0 in the effective superpotential. Combined with the effect of gaugino condensation in the hidden sector the total effective superpotential is then

$$W = W_0 + \sum_i A_i e^{-a_i T} \,. \tag{A.17}$$

For simplicity, let us assume a single condensate from the gauge group $\mathcal{G}_+$ with coefficients $A_+ = 1$ and $a = a_+$. To make contact with the notation of the previous section we need

merely identify[8]

$$a_+ \to \frac{3}{2b_+}\,. \tag{A.18}$$

Minimizing the resulting scalar potential $V(t,\bar{t})$ with $t = T|_{\theta=\bar{\theta}=0}$ generates a non-vanishing value for $\langle t+\bar{t}\rangle$ at which the auxiliary field F^T vanishes [60]. Restoring the Planck units to the second term in (A.8) we see that the vacuum must therefore have an energy density given by $\langle V\rangle = -3m_{3/2}^2 M_{\rm PL}^2$. The size of the VEV for $\mathrm{Re}\, t$, as well as the size of the gravitino mass $m_{3/2}$ are determined by the size of the constant term W_0 in (A.17). In particular we have [60]

$$\begin{aligned} \langle a_+ \mathrm{Re}\, t\rangle &\simeq \ln(1/W_0) \\ m_{3/2} &\simeq M_{\rm PL}\frac{W_0}{(2\,\langle \mathrm{Re}\, t\rangle)^{3/2}}\,. \end{aligned} \tag{A.19}$$

An acceptable phenomenology requires that the constant W_0 be finely-tuned to a value $W_0 \sim \mathcal{O}(10^{-13})$ in Planck units. That such a fine-tuning is possible at all is a particular feature of Type IIB compactifications with three-form fluxes. Combining the two relations in (A.19) we see that the model will assume an appropriate value of W_0 such that

$$\langle a_+ \mathrm{Re}\, t\rangle \simeq \ln(M_{\rm PL}/m_{3/2})\,. \tag{A.20}$$

The remaining component to the model is the sector that resolves the issue of the large negative vacuum energy. Here it is postulated that at the far tip of the Klebanov-Strassler throat there is an additional source of supersymmetry breaking. In this case we assume the presence of $\overline{D}_3$-branes which break supersymmetry *explicitly*. Being at the end of the warped throat the effect of this hard supersymmetry breaking is presumed to be mild on the observable sector D_7-branes. The vacuum stabilization for the Kähler modulus $t = T|_{\theta=\bar{\theta}=0}$ is thus largely unaffected. Being an explicit breaking of supersymmetry it is not possible to perfectly capture the effects of the $\overline{D}_3$-branes in the form of corrections to the supergravity effective Lagrangian in superspace. However, it can be approximated [38, 61] by assuming a correction to the pure-supergravity part of the action

$$\mathcal{L} \ni -2\int \mathrm{d}^4\theta E \to -2\int \mathrm{d}^4\theta\left[E + P(T,\overline{T})\right] \tag{A.21}$$

which gives rise to a new contribution to the scalar potential for the modulus T. When the modulus-dependence of $P(T,\overline{T})$ is trivial and $P(T,\overline{T}) = C$ then the resulting scalar potential contribution is simply

$$V_{\rm lift} = \frac{C}{(t+\bar{t})^2}\,, \tag{A.22}$$

and the more general case of $P(T,\overline{T}) = C(T+\overline{T})^n$ gives rise to

$$V_{\rm lift} = \frac{C}{(t+\bar{t})^{(2-n)}}\,. \tag{A.23}$$

[8] We have changed notation so as to ease comparisons with the original literature.

JHEP04(2009)114

Under these conditions the equations of motion for the auxiliary field for the Kähler modulus has the approximate solution

$$M_u = \left\langle \frac{F^T}{t+\bar{t}} \right\rangle \simeq m_{3/2} \frac{2-n}{a_+ \langle t+\bar{t} \rangle} \,. \tag{A.24}$$

To see how this generates a mirage pattern of masses, we look again at the ratio $r = M_g/M_u$

$$r = m_{3/2} \left\langle \frac{(t+\bar{t})}{F^T} \right\rangle = \frac{a_+ \langle t+\bar{t} \rangle}{2-n} \simeq \ln(M_{\rm PL}/m_{3/2}) \gg 1 \,. \tag{A.25}$$

Provided the VEVs in (A.19) can be arranged, the mirage pattern of gaugino masses necessarily follows. The implied value of α follows from the definition in (2.13)

$$\alpha = \frac{2}{2-n} + \mathcal{O}\left(\ln(m_{3/2}/M_{\rm PL})\right) \,. \tag{A.26}$$

In the minimal case with $n = 0$ we therefore have the prediction that $\alpha \simeq 1$ for this class of theories.

We note that in the case $n = 0$ we can rewrite the quantity r in (A.25) in the following way

$$r = a_+ \langle {\rm Re}\, t \rangle = a_+ \frac{1}{g^2_{\rm STR}} \quad \rightarrow \quad \frac{3}{2b_+ g^2_{\rm STR}} = \frac{\sqrt{3}}{2a_{\rm np}} \,. \tag{A.27}$$

Our two classes of theories are very different, yet they both result in a mirage pattern of gaugino masses in which the relative sizes of the contributions to soft supersymmetry breaking depend on the hidden sector gaugino condensation in a similar manner, as seen by their functional dependence on the parameters a_+ and/or b_+. Should we find this surprising? Perhaps not, since both aim to solve the same problem (namely, large negative vacuum energy) using the dynamics of a single real scalar field. And both methods ultimately involve adding a correction to the action for this real scalar of the form (A.21).[9] The *requirement* that $\langle V_{\rm total} \rangle = 0$ in the ground state then *dictates* the necessary values for the parameters such that the ratio $r = M_g/M_u$ dependence on the gaugino condensate is as in (A.27). We hasten to add, however, that the two models are indeed quite distinct in other regards. In particular they make quite different predictions for the other soft supersymmetry breaking parameters. For the case of the flux compactifications of Type IIB we refer the reader to the relevant literature [38, 62] for more details on how these additional terms are computed. We have chosen as a benchmark point a scenario studied in [38] in which $n = 0$ so that $\alpha = 1$. The overall scale was treated as a free parameter in [38] and we here take that scale to be $m_{3/2} = 16.3$ TeV. The precise values of the soft supersymmetry breaking parameters for both benchmark models are collected in table 1 in section 2 of the main text.

[9] Furthermore, in both constructions there are elements of this addition (A.21) that are not under full calculational control.

JHEP04(2009)114

B some statistical background material

As described in section 3.2, the method for determining a separation criterion for two models should be independent of the model in question or the signatures involved. Ultimately any such criterion should be determined solely by statistical considerations. In this appendix we describe how such an analytical expression can be derived.

Let us reconsider the quantum fluctuations. At a finite integrated luminosity L we can describe the outcome of a counting experiment as a Poisson distribution approximated by a normal distribution (this is a good approximation for approximately 10 counts or more), which can be expressed as

$$N_i = L\sigma_i + \sqrt{L\sigma_i}\, Z\,. \tag{B.1}$$

Here Z is a standard random variable, i.e. a random variable having a normal distribution centered at 0 with a standard deviation of 1. Note that by introducing statistical fluctuations via the variable Z we can replace $\bar{\sigma}_i$ in (B.1) with the exact cross section. Equation (B.1) then merely states the well known fact that the distribution in measured values N_i should form a normal distribution about the value $L\sigma_i$. To combine two such distributions N_1 and N_2 we may write

$$\begin{aligned} N_{\rm tot} &= \left(L\sigma_1 + \sqrt{L\sigma_1}Z_1\right) + \left(L\sigma_2 + \sqrt{L\sigma_2}Z_2\right) \\ &\equiv L\sigma^T + \sqrt{L\sigma^T}Z, \end{aligned} \tag{B.2}$$

where Z is a new standard random variable and σ^T is the total cross-section. For example, σ_1 might be the contribution to a particular final state arising from Standard Model processes while σ_2 might be the contribution arising from production of supersymmetric particles.

With the above in mind we can re-visit the definition (3.7) and obtain an analytic approximation for the distribution in $(\Delta S_{AB})^2$ values by using random variables to represent the signatures. The measured cross sections can be related to the exact cross sections via

$$\bar{\sigma}_i^A = N_i^A/L_A = \sigma_i^A + \sqrt{\sigma_i^A/L_A}\, Z_A\,, \tag{B.3}$$

with a similar expression for the model B. Substituting (B.3) into (3.7) gives

$$(\Delta S_{AB})^2 = \frac{1}{n}\sum_i \frac{\left[\sigma_i^A - \sigma_i^B + \sqrt{\frac{\sigma_i^A}{L_A}+\frac{\sigma_i^B}{L_B}}Z\right]^2}{\frac{\sigma_i^A}{L_A}+\frac{\sigma_i^B}{L_B}+\sqrt{\frac{1}{L_A^2}\frac{\sigma_i^A}{L^A}+\frac{1}{L_B^2}\frac{\sigma_i^B}{L^B}}Z'} \approx \frac{1}{n}\sum_i \left[\frac{\sigma_i^A-\sigma_i^B}{\sqrt{\frac{\sigma_i^A}{L_A}+\frac{\sigma_i^B}{L_B}}}+Z\right]^2\,, \tag{B.4}$$

where we have combined Z_A and Z_B into the random variables Z and Z' and have assumed that L_A and L_B are sufficiently large to be able to neglect the term proportional to Z'. In this limit we immediately see that $(\Delta S_{AB})^2$ is itself a random variable with a probability distribution for the quantity $(\Delta S_{AB})^2$ given by

$$P(\Delta S^2) = n\,\chi^2_{n,\lambda}(n\Delta S^2)\,, \tag{B.5}$$

JHEP04(2009)114

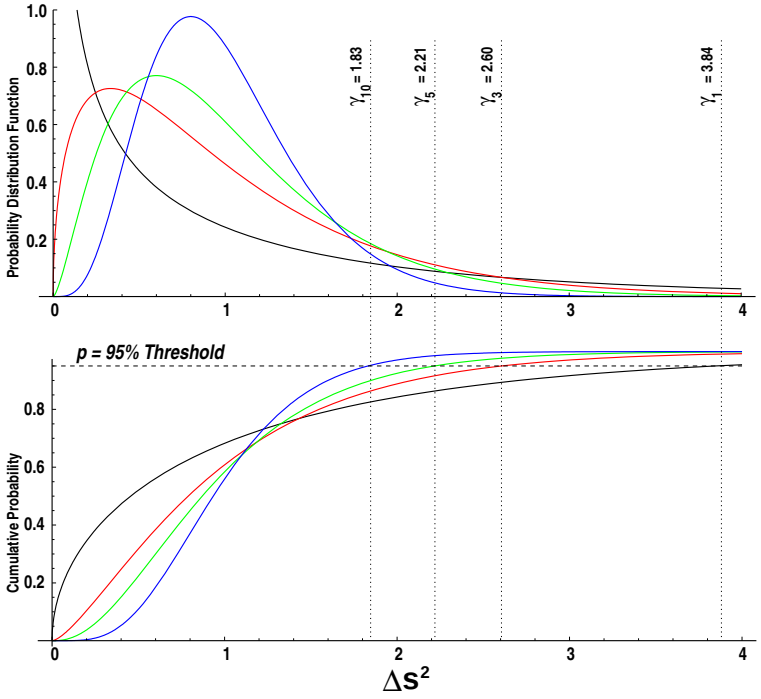

Figure 18. **Plot of distribution in $(\Delta S_{AA})^2$ values.** The top panel plots the probability distribution function (3.8) for $\lambda = 0$ and $n = 1$, 3, 5 and 10. The lower panel plots the cumulative distribution function — the absolute probability for obtaining that value of $(\Delta S)^2$. The 95% percent threshold is indicated by the horizontal lines, and the corresponding values of $(\Delta S)^2\big|_{95\text{th}}$ are indicated by the marked values of $\gamma_n(0.95)$.

where $\chi^2_{n,\lambda}$ is the non-central chi-squared distribution for n degrees of freedom.[10] The non-centrality parameter λ is given by

$$\lambda = \sum_i \frac{(\sigma_i^A - \sigma_i^B)^2}{\sigma_i^A/L_A + \sigma_i^B/L_B}\,, \tag{B.6}$$

and now the σ_i represent *exact* cross sections. This is actually the result we expect since the original $(\Delta S_{AB})^2$ in (3.7) is essentially a chi-square like function. Note that since the σ_i in the distribution of (B.4) are exact, we have the anticipated result that fluctuations of the quantity $(\Delta S_{AA})^2$ should be given by the central chi-square distribution $\chi^2_n(0)$. We note, however, that the derivation of (B.4) implicitly assumed that the signatures S_i which we consider are uncorrelated — or more precisely that the *fluctuations* in these signatures are uncorrelated. We now have a measure of separation in signature space that is related to well known functions in probability theory.[11]

[10] If we had chosen to define the separation variable (3.2) without the factor of $1/n$ we would have found that the distribution of $(\Delta S_{AB})^2$ values was exactly given by the non-central chi-square distribution. The two are related by a simple change of variables.

[11] In fact, the non-central chi-square distribution is related to the regularized confluent geometric functions .

JHEP04(2009)114

	Confidence Level p			
n	0.95	0.975	0.99	0.999
1	3.84	5.02	6.64	10.83
2	3.00	3.69	4.61	6.91
3	2.61	3.12	3.78	5.42
4	2.37	2.79	3.32	4.62
5	2.21	2.57	3.02	4.10
6	2.10	2.41	2.80	3.74
7	2.01	2.29	2.64	3.48
8	1.94	2.19	2.51	3.27
9	1.88	2.11	2.41	3.10
10	1.83	2.05	2.32	2.96

Table 10. **List of $\gamma_n(p)$ values for various values of the parameters n and p.** The value $\gamma_n(p)$ represents the position of the p-th percentile in the distribution of $P(\Delta S)^2$ for any list of n signatures. For example, if we consider a list of 10 signatures, then the quantity $(\Delta S_{AB})^2$ formed by these ten measurements must be larger than 1.83 to say that models A and B are distinct, with 95% confidence. If we demand 99% confidence this threshold becomes 2.32.

Armed with this technology, let us return to the issue of distinguishing a model from itself. The distribution of possible $(\Delta S_{AA})^2$ values (a central chi-square distribution) should depend *only* on the number n of signatures considered — not on the model point nor on the nature of those signatures. When comparing a model with itself we can therefore dispense with the subscript and write $(\Delta S_{AA})^2 = (\Delta S)^2$. We plot the probability distribution $P(\Delta S)^2$ of (B.5) for $\lambda = 0$ and various values of n in the top panel of figure 18. We have also plotted the cumulative distribution function for the same n values in the lower panel of figure 18. To rule out the null hypothesis (i.e. the hypothesis that models A and B are in fact the same model) to a level of confidence p requires demanding that $(\Delta S)^2$ is larger than the p-th percentile value for the distribution (B.5) for the appropriate n value. For example, if we use the criterion from [6] and require $(\Delta S_{AB})^2 > (\Delta S)^2\big|_{95\text{th}}$ then $p = 0.95$. We have indicated this value for the cumulative distribution function by the horizontal dashed line in figure 18. In general we will denote this particular value of $(\Delta S)^2\big|_p$ for each value of n by the symbol $\gamma_n(p)$. It can be found via the cumulative distribution function as in figure 18, or by numerically solving the equation

$$\Gamma\left(\frac{n}{2}, \frac{n}{2}\gamma_n(p)\right) = \Gamma\left(\frac{n}{2}\right)(1-p)\,, \tag{B.7}$$

where $\Gamma(n)$ is Euler's gamma function and $\Gamma(n,m)$ is the incomplete gamma function. A summary of these values for smaller n values is given in table 10. If we measure our n signatures, extract the cross-sections, form $(\Delta S_{AB})^2$ and the number is greater than $\gamma_n(p)$ then we can say that the null hypothesis can be ruled out at a level of confidence given by $p \times 100\%$. The value of this critical $(\Delta S)^2\big|_p = \gamma_n(p)$ is a universal number determined *only* by our choice of p value and the number of signatures n that we choose to consider.

If, however, our measurement gives $(\Delta S_{AB})^2 < \gamma_n(p)$ then we cannot say the two

JHEP04(2009)114

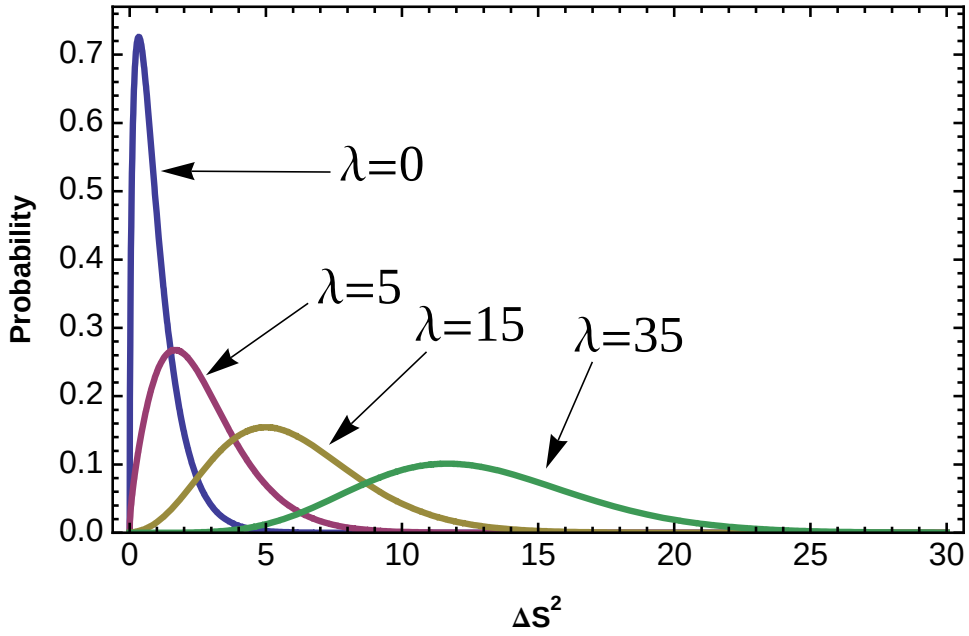

Figure 19. **Plot of distribution in $(\Delta S_{AB})^2$ values for $n = 3$ and various λ.** The probability distribution function (B.5) for $\lambda = 0$, 5, 15 and 35 is plotted for the case of $n = 3$. The curves are normalized such that the total area under each distribution remains unity. Note that the peak in the distribution moves to larger values of $(\Delta S_{AB})^2$ as the non-centrality parameter λ is increased.

models are distinct, at least not at the confidence level p. But they may still be separate models and we were simply unfortunate, with statistical fluctuations producing a small value of $(\Delta S_{AB})^2$. If we accumulate more data and measure $(\Delta S_{AB})^2$ again, we may find a different result. To quantify the probability that two different models A and B will give a particular value of $(\Delta S_{AB})^2$ requires the use of the non-central chi-square distribution in (B.5). The degree of non-centrality is given by the quantity λ in (B.6). Clearly, the more distinct the predictions σ_i^A and σ_i^B are from one another, the larger this number will be. In figure 19 we plot the distribution for $(\Delta S_{AB})^2$ for $n = 3$ signatures and several values of λ. As expected, the larger this parameter is, the more likely we are to find large values of $(\Delta S_{AB})^2$.

Let us assume for the moment that "model A" is the experimental data, which corresponds to an integrated luminosity of $L^{\rm exp}$. Our "model B" can then be a simulation with integrated luminosity $L^{\rm sim} = qL^{\rm exp}$. We might imagine that q can be arbitrarily large, limited only by computational resources.[12] We can then rewrite (B.6) as

$$\lambda = L^{\rm exp} \sum_i \frac{(\sigma_i^A - \sigma_i^B)^2}{\sigma_i^A + \frac{1}{q}\,\sigma_i^B}\,. \tag{B.8}$$

[12]Among other benefits of a large value for q would be the reduction in uncertainties arising from the simulation side of the comparison, i.e. assuming that the simulation perfectly captures both the physics and the detector response, the remaining uncertainty would be that associated with the experimental observation associated with σ_i^A.

JHEP04(2009)114

	Confidence Level p			
n	0.95	0.975	0.99	0.999
1	12.99	17.65	24.03	40.71
2	15.44	20.55	27.41	44.99
3	17.17	22.60	29.83	48.10
4	18.57	24.27	31.79	50.66
5	19.78	25.71	33.50	52.88
6	20.86	26.99	35.02	54.88
7	21.84	28.16	36.41	56.71
8	22.74	29.25	37.69	58.40
9	23.59	30.26	38.89	59.99
10	24.39	31.21	40.02	61.48

Table 11. **List of $\lambda_{\rm min}(n,p)$ values for various values of the parameters n and p.** A distribution such as those in figure 19 with $\lambda = \lambda_{\rm min}(n,p)$ will have precisely the fraction p of its total area at larger values of $(\Delta S_{AB})^2$ than the corresponding critical value $\gamma_n(p)$ from table 10. A graphical example of this statement is shown in figure 20.

From this expression it is clear that we can expect the value of this parameter λ to *increase* as experimental data is collected. The larger the value of $L^{\rm exp}$ the less likely it becomes to find a particularly small value of $(\Delta S_{AB})^2$. This confirms out basic intuition that given *any* observable (or set of observables) for which the two models predict different values then with sufficient integrated luminosity it should always be possible to distinguish the models to arbitrary degree of confidence.

For any given value of $\lambda \neq 0$, the probability that a measurement of $(\Delta S_{AB})^2$ will fluctuate to a value so small that it is not possible to separate two distinct models (to confidence level p) is simply the fraction of the probability distribution in (B.5) that lies to the left of the value $\gamma_n(p)$. If we wish to be at least 95% certain that our measurements will correctly recognize that two different models are indeed distinct we must require

$$P = \int_{\gamma_n(p)}^{\infty} n\,\chi^2_{n,\lambda}(n\Delta S^2_{AB})\,d(\Delta S^2_{AB}) = \int_{n\gamma_n(p)}^{\infty} \chi^2_{n,\lambda}(y)\,dy \geq 0.95\,. \tag{B.9}$$

Since the value of the integral P in (B.9) decreases monotonically as λ increases the value of this parameter which makes (B.9) an equality is the minimum non-centrality value $\lambda_{\rm min}(n,p)$ such that the two models can be distinguished.

In other words for two distinct models A and B, any combination of n experimental signatures such that $\lambda > \lambda_{\rm min}(n, p = 0.95)$ will be effective in demonstrating that the two models are indeed different 95% of the time, with a confidence level of 95%. We have successfully reduced the problem to an exercise in pure mathematics, as these $\lambda_{\rm min}(n,p)$ values can be calculated analytically without regard to the physics involved. A collection of values for small values of n are given in table 11. Note that as we increase n the necessary value $\lambda_{\rm min}$ increases, reflecting the fact that as more observations are made we should expect that it will become increasingly likely that at least one will show a large deviation. Indeed, the quantity λ can be thought of as a measure of the overall distance from $(\Delta S_{AB})^2 = 0$ in

JHEP04(2009)114

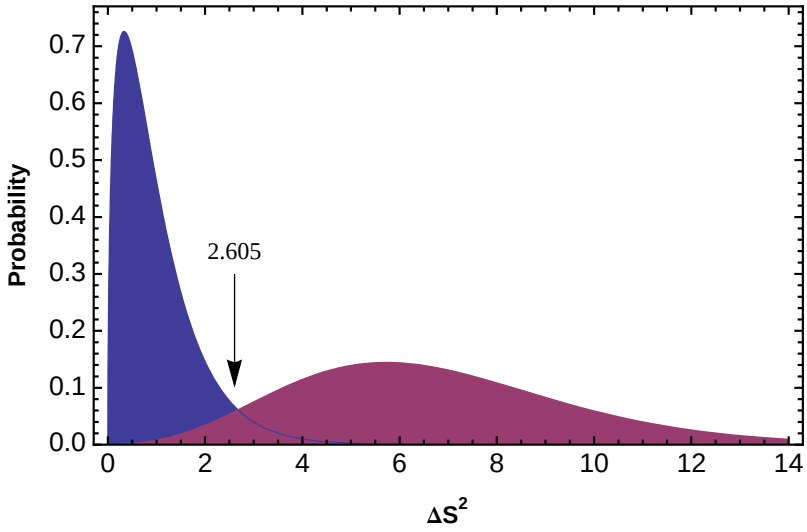

Figure 20. **Determination of $\lambda_{\min}$ for the case $n = 3$.** The plot shows an example of the distribution of $(\Delta S_{AB})^2$ for $n = 3$. The curve on the left represent $\lambda = 0$ case, i.e. values we will get when we compare a model to itself. 95% of the possible outcomes of this comparison are below 2.61 which is shown on the plot. The curve on the right has $\lambda = 17.17$ and 95% of the curve is beyond 2.61. As λ increases, this curve moves further to the right and gets flatter.

the n-dimensional signature space in units of the variances. As an example, again consider the case where $n = 3$. For this value of n the corresponding $\gamma_3(0.95) = 2.61$ value can be found from table 10, while we can find $\lambda_{\min}(3, 0.95) = 17.17$ from table 11. We plot the distributions (3.8) for $\{n, \lambda\} = \{3, 0\}$ and $\{3, 17.17\}$ simultaneously in figure 20. By construction, the area of the non-central distribution to the left of the indicated value of $(\Delta S_{AB})^2 = 2.61$ will be precisely 5% of the total area.

We have successfully reduced the problem to an exercise in pure mathematics, as these $\lambda_{\min}(n, p)$ values can be calculated analytically without regard to the physics involved. A collection of values for small values of n are given in table 11. Note that as we increase n the necessary value $\lambda_{\min}$ increases, reflecting the fact that as more observations are made we should expect that it will become increasingly likely that at least one will show a large deviation. Indeed, the quantity λ can be thought of as a measure of the overall distance from $(\Delta S_{AB})^2 = 0$ in the n-dimensional signature space in units of the variances. As an example, again consider the case where $n = 3$. For this value of n the corresponding $\gamma_3(0.95) = 2.61$ value can be found from table 10, while we can find $\lambda_{\min}(3, 0.95) = 17.17$ from table 11. We plot the distributions (3.8) for $\{n, \lambda\} = \{3, 0\}$ and $\{3, 17.17\}$ simultaneously in figure 20. By construction, the area of the non-central distribution to the left of the indicated value of $(\Delta S_{AB})^2 = 2.61$ will be precisely 5% of the total area.

References

[1] See, for example, G.F. Giudice, *Theories for the Fermi scale*, *J. Phys. Conf. Ser.* **110** (2008) 012014 [arXiv:0710.3294] [SPIRES];

JHEP04(2009)114

G.H. Brooijmans et al., *New physics at the LHC: a Les Houches report. Physics at TeV colliders* 2007 – *New physics working group*, arXiv:0802.3715 [SPIRES];
M. Fairbairn et al., *Stable massive particles at colliders*, *Phys. Rept.* **438** (2007) 1 [hep-ph/0611040] [SPIRES].

[2] G.L. Kane, J.D. Lykken, B.D. Nelson and L.-T. Wang, *Re-examination of electroweak symmetry breaking in supersymmetry and implications for light superpartners*, *Phys. Lett.* **B 551** (2003) 146 [hep-ph/0207168] [SPIRES].

[3] G.L. Kane, A.A. Petrov, J. Shao and L.-T. Wang, *Initial determination of the spins of the gluino and squarks at LHC*, arXiv:0805.1397 [SPIRES].

[4] J. Hubisz, J. Lykken, M. Pierini and M. Spiropulu, *Missing energy look-alikes with* $100\,pb^{-1}$ *at the LHC*, *Phys. Rev.* **D 78** (2008) 075008 [arXiv:0805.2398] [SPIRES].

[5] ATLAS collaboration, S. Yamamoto, *Strategy for early SUSY searches at ATLAS*, arXiv:0710.3953 [SPIRES].

[6] N. Arkani-Hamed, G.L. Kane, J. Thaler and L.-T. Wang, *Supersymmetry and the LHC inverse problem*, *JHEP* **08** (2006) 070 [hep-ph/0512190] [SPIRES].

[7] G.L. Kane, P. Kumar, D.E. Morrissey and M. Toharia, *Connecting (supersymmetry) LHC measurements with high scale theories*, *Phys. Rev.* **D 75** (2007) 115018 [hep-ph/0612287] [SPIRES].

[8] C.F. Berger, J.S. Gainer, J.L. Hewett, T.G. Rizzo and B. Lillie, *The LHC inverse problem, supersymmetry and the ILC*, arXiv:0711.1374 [SPIRES].

[9] C.F. Berger, J.S. Gainer, J.L. Hewett, B. Lillie and T.G. Rizzo, *General features of supersymmetric signals at the ILC: solving the LHC inverse problem*, arXiv:0712.2965 [SPIRES].

[10] B. Altunkaynak, M. Holmes and B.D. Nelson, *Solving the LHC inverse problem with dark matter observations*, *JHEP* **10** (2008) 013 [arXiv:0804.2899] [SPIRES].

[11] G. Kane and S. Watson, *Dark matter and LHC: what is the connection?*, *Mod. Phys. Lett.* **A 23** (2008) 2103 [arXiv:0807.2244] [SPIRES].

[12] P. Binetruy, G.L. Kane, B.D. Nelson, L.-T. Wang and T.T. Wang, *Relating incomplete data and incomplete theory*, *Phys. Rev.* **D 70** (2004) 095006 [hep-ph/0312248] [SPIRES].

[13] B.C. Allanach, K. Cranmer, C.G. Lester and A.M. Weber, *Natural priors, CMSSM fits and LHC weather forecasts*, *JHEP* **08** (2007) 023 [arXiv:0705.0487] [SPIRES];
B.C. Allanach, *Naturalness priors and fits to the constrained minimal supersymmetric standard model*, *Phys. Lett.* **B 635** (2006) 123 [hep-ph/0601089] [SPIRES];
B.C. Allanach and C.G. Lester, *Multi-Dimensional mSUGRA likelihood maps*, *Phys. Rev.* **D 73** (2006) 015013 [hep-ph/0507283] [SPIRES];
J.R. Ellis, S. Heinemeyer, K.A. Olive, A.M. Weber and G. Weiglein, *The supersymmetric parameter space in light of* B^- *physics observables and electroweak precision data*, *JHEP* **08** (2007) 083 [arXiv:0706.0652] [SPIRES];
R.R. de Austri, R. Trotta and L. Roszkowski, *A Markov chain Monte Carlo analysis of the CMSSM*, *JHEP* **05** (2006) 002 [hep-ph/0602028] [SPIRES];
L. Roszkowski, R. Ruiz de Austri and R. Trotta, *Implications for the Constrained MSSM from a new prediction for* $b \to s\gamma$, *JHEP* **07** (2007) 075 [arXiv:0705.2012] [SPIRES];
J.R. Ellis, S. Heinemeyer, K.A. Olive and G. Weiglein, *Phenomenological indications of the scale of supersymmetry*, *JHEP* **05** (2006) 005 [hep-ph/0602220] [SPIRES].

JHEP04(2009)114

[14] M. Brhlik and G.L. Kane, *Measuring the supersymmetry Lagrangian*, *Phys. Lett.* **B 437** (1998) 331 [hep-ph/9803391] [SPIRES].

[15] P. Nath and T.R. Taylor, *Modular invariance, soft breaking, mu and* $\tan\beta$ *in superstring models*, *Phys. Lett.* **B 548** (2002) 77 [hep-ph/0209282] [SPIRES].

[16] G.F. Giudice and A. Masiero, *A natural solution to the* μ *problem in supergravity theories*, *Phys. Lett.* **B 206** (1988) 480 [SPIRES].

[17] P. Binetruy, G.L. Kane, J.D. Lykken and B.D. Nelson, *Twenty-five questions for string theorists*, *J. Phys.* **G 32** (2006) 129 [hep-th/0509157] [SPIRES].

[18] J.L. Kneur and G. Moultaka, *Inverting the supersymmetric standard model spectrum: from physical to lagrangian ino parameters*, *Phys. Rev.* **D 59** (1999) 015005 [hep-ph/9807336] [SPIRES].

[19] S.P. Martin and M.T. Vaughn, *Regularization dependence of running couplings in softly broken supersymmetry*, *Phys. Lett.* **B 318** (1993) 331 [hep-ph/9308222] [SPIRES].

[20] N.V. Krasnikov, *The Relation between pole and running masses for gluino and squarks*, *Phys. Lett.* **B 345** (1995) 25 [SPIRES].

[21] R.L. Arnowitt and P. Nath, *SUSY mass spectrum in* SU(5) *supergravity grand unification*, *Phys. Rev. Lett.* **69** (1992) 725 [SPIRES].

[22] S. Bhattacharya, A. Datta and B. Mukhopadhyaya, *Non-universal gaugino masses: a signal-based analysis for the Large Hadron Collider*, *JHEP* **10** (2007) 080 [arXiv:0708.2427] [SPIRES].

[23] S. Bhattacharya, A. Datta and B. Mukhopadhyaya, *Non-universal gaugino and scalar masses, hadronically quiet trileptons and the Large Hadron Collider*, *Phys. Rev.* **D 78** (2008) 115018 [arXiv:0809.2012] [SPIRES].

[24] K. Choi and H.P. Nilles, *The gaugino code*, *JHEP* **04** (2007) 006 [hep-ph/0702146] [SPIRES].

[25] G.F. Giudice, M.A. Luty, H. Murayama and R. Rattazzi, *Gaugino mass without singlets*, *JHEP* **12** (1998) 027 [hep-ph/9810442] [SPIRES].

[26] L. Randall and R. Sundrum, *Out of this world supersymmetry breaking*, *Nucl. Phys.* **B 557** (1999) 79 [hep-th/9810155] [SPIRES].

[27] S. Kachru, R. Kallosh, A. Linde and S.P. Trivedi, *De Sitter vacua in string theory*, *Phys. Rev.* **D 68** (2003) 046005 [hep-th/0301240] [SPIRES].

[28] M. Graña, *Flux compactifications in string theory: a comprehensive review*, *Phys. Rept.* **423** (2006) 91 [hep-th/0509003] [SPIRES].

[29] M.K. Gaillard and B.D. Nelson, *Kähler stabilized, modular invariant heterotic string models*, *Int. J. Mod. Phys.* **A 22** (2007) 1451 [hep-th/0703227] [SPIRES].

[30] L.L. Everett, I.-W. Kim, P. Ouyang and K.M. Zurek, *Deflected mirage mediation: a framework for generalized supersymmetry breaking*, *Phys. Rev. Lett.* **101** (2008) 101803 [arXiv:0804.0592] [SPIRES].

[31] L.L. Everett, I.-W. Kim, P. Ouyang and K.M. Zurek, *Moduli stabilization and supersymmetry breaking in deflected mirage mediation*, *JHEP* **08** (2008) 102 [arXiv:0806.2330] [SPIRES].

JHEP04(2009)114

[32] E. Katz, Y. Shadmi and Y. Shirman, *Heavy thresholds, slepton masses and the μ term in anomaly mediated supersymmetry breaking*, *JHEP* **08** (1999) 015 [hep-ph/9906296] [SPIRES].

[33] R. Rattazzi, A. Strumia and J.D. Wells, *Phenomenology of deflected anomaly mediation*, *Nucl. Phys.* **B 576** (2000) 3 [hep-ph/9912390] [SPIRES].

[34] T. Gherghetta, G.F. Giudice and J.D. Wells, *Phenomenological consequences of supersymmetry with anomaly-induced masses*, *Nucl. Phys.* **B 559** (1999) 27 [hep-ph/9904378] [SPIRES];
J.L. Feng, T. Moroi, L. Randall, M. Strassler and S.-F. Su, *Discovering supersymmetry at the Tevatron in Wino LSP scenarios*, *Phys. Rev. Lett.* **83** (1999) 1731 [hep-ph/9904250] [SPIRES];
A.J. Barr, C.G. Lester, M.A. Parker, B.C. Allanach and P. Richardson, *Discovering anomaly-mediated supersymmetry at the LHC*, *JHEP* **03** (2003) 045 [hep-ph/0208214] [SPIRES];
M. Ibe, T. Moroi and T.T. Yanagida, *Possible signals of Wino LSP at the Large Hadron Collider*, *Phys. Lett.* **B 644** (2007) 355 [hep-ph/0610277] [SPIRES];
S. Asai, T. Moroi, K. Nishihara and T.T. Yanagida, *Testing the anomaly mediation at the LHC*, *Phys. Lett.* **B 653** (2007) 81 [arXiv:0705.3086] [SPIRES];
S. Asai, T. Moroi and T.T. Yanagida, *Test of anomaly mediation at the LHC*, *Phys. Lett.* **B 664** (2008) 185 [arXiv:0802.3725] [SPIRES].

[35] M.K. Gaillard, B.D. Nelson and Y.Y. Wu, *Gaugino masses in modular invariant supergravity*, *Phys. Lett.* **B 459** (1999) 549 [hep-th/9905122] [SPIRES].

[36] J.A. Bagger, T. Moroi and E. Poppitz, *Anomaly mediation in supergravity theories*, *JHEP* **04** (2000) 009 [hep-th/9911029] [SPIRES].

[37] G.L. Kane et al., *Theory-motivated benchmark models and superpartners at the Tevatron*, *Phys. Rev.* **D 67** (2003) 045008 [hep-ph/0209061] [SPIRES].

[38] K. Choi, K.S. Jeong and K.-I. Okumura, *Phenomenology of mixed modulus-anomaly mediation in fluxed string compactifications and brane models*, *JHEP* **09** (2005) 039 [hep-ph/0504037] [SPIRES].

[39] B.C. Allanach et al., *The Snowmass points and slopes: benchmarks for SUSY searches*, in the proceedings of the *APS/DPF/DPB Summer Study on the Future of Particle Physics (Snowmass2001)*, June 30–July 21, Snowmass, Colorado U.S.A. (2001), N. Graf ed., *Eur. Phys. J.* **C 25** (2002) 113 [hep-ph/0202233] [SPIRES].

[40] T. Sjöstrand, S. Mrenna and P. Skands, *PYTHIA* 6.4 *physics and manual*, *JHEP* **05** (2006) 026 [hep-ph/0603175] [SPIRES].

[41] See http://www.physics.ucdavis.edu/~conway/research/software/pgs/pgs4-general.htm.

[42] D. Feldman, Z. Liu and P. Nath, *Sparticles at the LHC*, *JHEP* **04** (2008) 054 [arXiv:0802.4085] [SPIRES].

[43] ATLAS AND CMS collaboration, J.G. Branson et al., *High transverse momentum physics at the Large Hadron Collider: the ATLAS and CMS collaborations*, *Eur. Phys. J. direct* **C 4** (2002) N1 [hep-ph/0110021] [SPIRES];
H. Baer, X. Tata and J. Woodside, *Multi-lepton signals from supersymmetry at hadron super colliders*, *Phys. Rev.* **D 45** (1992) 142 [SPIRES];

JHEP04(2009)114

H. Baer, C.-H. Chen, F. Paige and X. Tata, *Trileptons from chargino-neutralino production at the CERN Large Hadron Collider*, *Phys. Rev.* **D 50** (1994) 4508 [hep-ph/9404212] [SPIRES]; *Signals for minimal supergravity at the CERN Large Hadron Collider: multi-jet plus missing energy channel*, *Phys. Rev.* **D 52** (1995) 2746 [hep-ph/9503271] [SPIRES]; *Signals for minimal supergravity at the CERN Large Hadron Collider II: multilepton channels*, *Phys. Rev.* **D 53** (1996) 6241 [hep-ph/9512383] [SPIRES];
I. Hinchliffe, F.E. Paige, M.D. Shapiro, J. Soderqvist and W. Yao, *Precision SUSY measurements at CERN LHC*, *Phys. Rev.* **D 55** (1997) 5520 [hep-ph/9610544] [SPIRES].

[44] See http://www.atsweb.neu.edu/ialtunkaynak/heptools.html#parvicursor.

[45] A. Djouadi, J.-L. Kneur and G. Moultaka, *SuSpect: a Fortran code for the supersymmetric and Higgs particle spectrum in the MSSM*, *Comput. Phys. Commun.* **176** (2007) 426 [hep-ph/0211331] [SPIRES].

[46] A. Djouadi, M.M. Muhlleitner and M. Spira, *Decays of supersymmetric particles: the program SUSY-HIT (SUspect-SdecaY-HDECAY-InTerface)*, *Acta Phys. Polon.* **B 38** (2007) 635 [hep-ph/0609292] [SPIRES].

[47] J.L. Bourjaily, G.L. Kane, P. Kumar and T.T. Wang, *Outside the mSUGRA box*, hep-ph/0504170 [SPIRES].

[48] G.L. Kane, P. Kumar and J. Shao, *LHC string phenomenology*, *J. Phys.* **G 34** (2007) 1993 [hep-ph/0610038] [SPIRES].

[49] G.L. Kane, P. Kumar and J. Shao, *Unravelling strings at the LHC*, *Phys. Rev.* **D 77** (2008) 116005 [arXiv:0709.4259] [SPIRES].

[50] N. Arkani-Hamed et al., *MARMOSET: the path from LHC data to the new standard model via on-shell effective theories*, hep-ph/0703088 [SPIRES].

[51] P. Binetruy, M.K. Gaillard and B.D. Nelson, *One loop soft supersymmetry breaking terms in superstring effective theories*, *Nucl. Phys.* **B 604** (2001) 32 [hep-ph/0011081] [SPIRES].

[52] A. Brignole, L.E. Ibáñez and C. Muñoz, *Towards a theory of soft terms for the supersymmetric standard model*, *Nucl. Phys.* **B 422** (1994) 125 [*Erratum ibid.* **B 436** (1995) 747] [hep-ph/9308271] [SPIRES].

[53] P. Binetruy, M.K. Gaillard and Y.-Y. Wu, *Dilaton stabilization in the context of dynamical supersymmetry breaking through gaugino condensation*, *Nucl. Phys.* **B 481** (1996) 109 [hep-th/9605170] [SPIRES].

[54] P. Binetruy, M.K. Gaillard and Y.-Y. Wu, *Modular invariant formulation of multi-gaugino and matter condensation*, *Nucl. Phys.* **B 493** (1997) 27 [hep-th/9611149] [SPIRES].

[55] S.H. Shenker, *The strength of nonperturbative effects in string theory*, presented at the *Cargese workshop on random surfaces, Quantum Gravity and Strings*, May 28–June 1, Cargese, France (1990), RU-90-47 [SPIRES].

[56] J.A. Casas, *The generalized dilaton supersymmetry breaking scenario*, *Phys. Lett.* **B 384** (1996) 103 [hep-th/9605180] [SPIRES].

[57] P. Binetruy, M.K. Gaillard and Y.-Y. Wu, *Supersymmetry breaking and weakly vs. strongly coupled string theory*, *Phys. Lett.* **B 412** (1997) 288 [hep-th/9702105] [SPIRES].

[58] M.K. Gaillard and B.D. Nelson, *Constraints on hidden sector gaugino condensation*, *Nucl. Phys.* **B 571** (2000) 3 [hep-ph/9909563] [SPIRES].

JHEP04(2009)114

[59] I.R. Klebanov and M.J. Strassler, *Supergravity and a confining gauge theory: duality cascades and χ_{SB}-resolution of naked singularities*, *JHEP* **08** (2000) 052 [hep-th/0007191] [SPIRES].

[60] K. Choi, A. Falkowski, H.P. Nilles, M. Olechowski and S. Pokorski, *Stability of flux compactifications and the pattern of supersymmetry breaking*, *JHEP* **11** (2004) 076 [hep-th/0411066] [SPIRES].

[61] K. Choi, A. Falkowski, H.P. Nilles and M. Olechowski, *Soft supersymmetry breaking in KKLT flux compactification*, *Nucl. Phys.* **B 718** (2005) 113 [hep-th/0503216] [SPIRES].

[62] A. Falkowski, O. Lebedev and Y. Mambrini, *SUSY phenomenology of KKLT flux compactifications*, *JHEP* **11** (2005) 034 [hep-ph/0507110] [SPIRES].

JHEP04(2009)114